

# 1 Efficient N<sub>2</sub>O<sub>5</sub> Uptake and NO<sub>3</sub> Oxidation in the Outflow of Urban Beijing

2 Haichao Wang<sup>1</sup>, Keding Lu<sup>1\*</sup>, Song Guo<sup>1</sup>, Zhijun Wu<sup>1</sup>, Dongjie Shang<sup>1</sup>, Zhaofeng Tan<sup>1</sup>, Yujue Wang<sup>1</sup>,  
3 Michael Le Breton<sup>2</sup>, Shengrong Lou<sup>3</sup>, Mingjin Tang<sup>4</sup>, Yusheng Wu<sup>1</sup>, Jing Zheng<sup>1</sup>, Limin Zeng<sup>1</sup>,  
4 Mattias Hallquist<sup>2</sup>, Min Hu<sup>1</sup> and Yuanhang Zhang<sup>1, 5</sup>

5

6 <sup>1</sup>State Key Joint Laboratory of Environmental Simulation and Pollution Control, College of  
7 Environmental Sciences and Engineering, Peking University, Beijing, China.

8 <sup>2</sup>Department of Chemistry and Molecular Biology, University of Gothenburg, Gothenburg, Sweden

9 <sup>3</sup>Shanghai Academy of Environmental Sciences, Shanghai, China

10 <sup>4</sup>State Key Laboratory of Organic Geochemistry and Guangdong Key Laboratory of Environmental  
11 Protection and Resources Utilization, Guangzhou Institute of Geochemistry, Chinese Academy of  
12 Sciences, Guangzhou, China

13 <sup>5</sup>CAS Center for Excellence in Regional Atmospheric Environment, Chinese Academy of Sciences,  
14 Xiamen, China

15

16 \*Corresponding to: Keding Lu ([k.lu@pku.edu.cn](mailto:k.lu@pku.edu.cn))

17

18 **Abstract.** Nocturnal reactive nitrogen compounds play an important role in regional air pollution. Here  
19 we present the measurements of dinitrogen pentoxide (N<sub>2</sub>O<sub>5</sub>) associated with nitryl chloride (ClNO<sub>2</sub>)  
20 and particulate nitrate (pNO<sub>3</sub><sup>-</sup>) in a suburban site of Beijing in the summer of 2016. High levels of  
21 N<sub>2</sub>O<sub>5</sub> and ClNO<sub>2</sub> were observed in the outflow of the urban Beijing air masses, with 1-min average  
22 maxima of 937 pptv and 2900 pptv, respectively. The N<sub>2</sub>O<sub>5</sub> uptake coefficients,  $\gamma$ , and ClNO<sub>2</sub> yield,  $f$ ,  
23 were experimentally determined from the observed parameters. The N<sub>2</sub>O<sub>5</sub> uptake coefficient ranged  
24 from 0.012 to 0.055, with an average of  $0.034 \pm 0.018$ , which is in the upper range of previous field  
25 studies reported in North America and Europe but is a moderate value in the North China Plain (NCP),  
26 which reflects efficient N<sub>2</sub>O<sub>5</sub> heterogeneous processes in Beijing. The ClNO<sub>2</sub> yield exhibited high  
27 variability, with a range of 0.50 to unity and an average of  $0.73 \pm 0.25$ . The concentration of the nitrate  
28 radical (NO<sub>3</sub>) was calculated assuming that the thermal equilibrium between NO<sub>3</sub> and N<sub>2</sub>O<sub>5</sub> was  
29 maintained. In NO<sub>x</sub>-rich air masses, the oxidation of nocturnal biogenic volatile organic compounds  
30 (BVOCs) was dominated by NO<sub>3</sub> rather than O<sub>3</sub>. The production rate of organic nitrate (ON) via  
31 NO<sub>3</sub>+BVOCs was significant, with an average of  $0.10 \pm 0.07$  ppbv h<sup>-1</sup>. We highlight the importance  
32 of NO<sub>3</sub> oxidation of VOCs in the formation of ON and subsequent secondary organic aerosols in  
33 summer in Beijing.

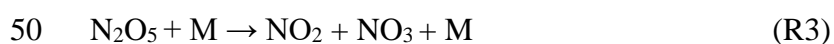
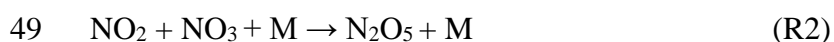
34

35

36

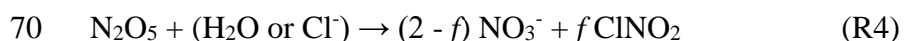
## 37 1. Introduction

38 It has been well recognized that reactive nitrogen compounds, specifically the nitrate radical (NO<sub>3</sub>)  
39 and dinitrogen pentoxide (N<sub>2</sub>O<sub>5</sub>), play a key role in nighttime chemistry (Wayne et al., 1991; Brown  
40 and Stutz, 2012). NO<sub>3</sub> is the most important oxidant in the nighttime and can be considered the  
41 nighttime analogue of the hydroxyl radical (OH) for certain VOCs (Wayne et al., 1991; Benton et al.,  
42 2010). NO<sub>3</sub> can initiate the removal of many kind of anthropogenic and biogenic emissions after sunset.  
43 In NO<sub>x</sub>-rich plumes, NO<sub>3</sub> is responsible for the vast majority of the oxidation of biogenic VOCs  
44 because of its rapid reactions with unsaturated hydrocarbons (Edwards et al., 2017). NO<sub>3</sub> is  
45 predominantly formed by the reaction of NO<sub>2</sub> with O<sub>3</sub> (R1) and further reacts with NO<sub>2</sub> to produce  
46 N<sub>2</sub>O<sub>5</sub> (R2). N<sub>2</sub>O<sub>5</sub> is rapidly decomposed back to NO<sub>3</sub> (R3), NO<sub>3</sub> and N<sub>2</sub>O<sub>5</sub> are in dynamic equilibrium  
47 in the troposphere.



51 Photolysis of NO<sub>3</sub> and the reaction of NO<sub>3</sub> with NO are rapid, which lead to a daytime NO<sub>3</sub> lifetime  
52 being shorter than 5 s with extremely low concentrations, whereas in low-NO air masses, the fate of  
53 NO<sub>3</sub> is mainly controlled by the mixing ratios of various VOCs and N<sub>2</sub>O<sub>5</sub> heterogeneous hydrolysis  
54 because the two terms are the dominating loss pathways of NO<sub>3</sub> and N<sub>2</sub>O<sub>5</sub>. The VOCs reaction is  
55 significant downwind of an urban area or a strongly urban-influenced forested area in summer. The  
56 NO<sub>3</sub> oxidation of VOCs was responsible for more than 70% nocturnal NO<sub>3</sub> loss in Houston (Stutz et  
57 al., 2010) and contributed approximately 50% in the forest region in Germany (Geyer et al., 2001).  
58 The reactions of NO<sub>3</sub> with several BVOCs produce considerable amounts of organic nitrates (ON)  
59 with efficient yields, which act as important precursors of secondary organic aerosols (SOA). The  
60 reaction of NO<sub>3</sub> with isoprene has a SOA mass yield of 23.8% (Ng et al., 2008). For the reaction with  
61 monoterpene, such as limonene, the SOA mass yield can reach 174% at ambient temperatures (Boyd  
62 et al., 2017). The reactions of NO<sub>3</sub>+BVOCs are critical to the studies of aerosols on regional and global  
63 scales (Fry et al., 2009; Rollins et al., 2009; Pye et al., 2010; Ng et al., 2017). For example, ON had  
64 extensive percentages of fine particulate nitrate (pNO<sub>3</sub><sup>-</sup>) (34% - 44%) in Europe (Kiendler-Scharr et  
65 al., 2016).

66 The heterogeneous hydrolysis of N<sub>2</sub>O<sub>5</sub> produces soluble nitrate (HNO<sub>3</sub> or NO<sub>3</sub><sup>-</sup>) and nitryl chloride  
67 (ClNO<sub>2</sub>) on chloride-containing aerosols (R4) (Finlayson-Pitts et al., 1989). This reaction is known to  
68 be an important intermediate in the NO<sub>x</sub> removal processes (Brown et al., 2006). The pseudo-first order  
69 loss rate constant of N<sub>2</sub>O<sub>5</sub> via heterogeneous uptake is given in Eq. 1 (Wahner et al., 1998).



$$71 k_{\text{N}_2\text{O}_5} = 0.25 \cdot c \cdot \gamma(\text{N}_2\text{O}_5) \cdot S_a \quad (\text{Eq. 1})$$

72 Where  $c$  is the mean molecule speed of N<sub>2</sub>O<sub>5</sub>,  $S_a$  is the aerosol surface concentration and  $\gamma(\text{N}_2\text{O}_5)$  is  
73 the N<sub>2</sub>O<sub>5</sub> uptake coefficient. N<sub>2</sub>O<sub>5</sub> heterogeneous hydrolysis is one of the major uncertainties of the  
74 NO<sub>3</sub> budget since the N<sub>2</sub>O<sub>5</sub> uptake coefficient can be highly variable and difficult to quantify (Brown  
75 and Stutz, 2012; Chang et al., 2011; H. C. Wang et al., 2016). Laboratory and field measurement studies

76 have reported that the  $\text{N}_2\text{O}_5$  uptake coefficient has large variability and ranges from  $<0.001$  to  $0.1$ ; the  
77  $\text{N}_2\text{O}_5$  uptake coefficient depends on relative humidity (RH), particle morphology, compositions (water  
78 content, nitrate, sulfate, organic or mineral particles) and other factors (Wahner et al., 1998; Mentel et  
79 al., 1999; Hallquist et al., 2003; Thornton et al., 2003; Thornton et al., 2005; Brown et al., 2006;  
80 Bertram and Thornton, 2009; Tang et al., 2012, 2014; Gaston et al., 2014; Grzanic et al., 2015; Tang et  
81 al., 2017). The coupled chemical mechanisms in ambient conditions are still not well understood.  
82  $\text{ClNO}_2$  forms and accumulates with a negligible sink during the night and further photolyzes and  
83 liberates the chlorine radical (Cl) and  $\text{NO}_2$  after sunrise. Hundreds of pptv to ppbv of  $\text{ClNO}_2$  can lead  
84 to several ppbv of  $\text{O}_3$  enhancement and significant primary  $\text{RO}_x$  production (Osthoff et al., 2008;  
85 Thornton et al., 2010; McLaren et al., 2010; Riedel et al., 2014; Sarwar et al., 2014; Tham et al., 2016).

86 Large amounts of  $\text{NO}_x$  have been emitted for the past several decades in China, but comprehensive  
87 field studies of the nighttime chemical processes of reactive nitrogen oxides remain sparse. Previous  
88 studies have found high mixing ratios of  $\text{NO}_3$  associated with high  $\text{NO}_3$  reactivity in the megacities in  
89 China, including Shanghai, the Pearl River Delta (PRD) and Beijing (Li et al., 2012; Wang et al., 2013;  
90 Wang et al., 2015). The  $\text{N}_2\text{O}_5$  concentration was elevated in Beijing (H. C. Wang et al., 2017a; H. C.  
91 Wang et al., 2017c) but was moderate in other places of North China Plain (NCP), such as Wangdu,  
92 Jinan and Mount Tai (Tham et al., 2016; X. F. Wang et al., 2017; Z. Wang et al., 2017). Recently, the  
93  $\text{N}_2\text{O}_5$  uptake coefficients were determined to be very high, even up to  $0.1$  in NCP, but the reason is still  
94 not well studied (H. C. Wang et al., 2017c; X. F. Wang et al., 2017; Z. Wang et al., 2017). Reactive  
95  $\text{N}_2\text{O}_5$  chemistry was also reported in Hong Kong, and showed the highest field-observed  $\text{N}_2\text{O}_5$   
96 concentration to date (T. Wang et al., 2016; Brown et al., 2016). Observations and model simulations  
97 revealed that fast heterogeneous uptake of  $\text{N}_2\text{O}_5$  is an important pathway of  $\text{pNO}_3^-$  formation in China  
98 (H. C. Wang et al., 2017b; H. C. Wang et al., 2017c; Z. Wang et al., 2017; Su et al., 2017); the reaction  
99 also contributed significantly to removal (Z. Wang et al., 2017; Brown et al., 2016). Moreover, chlorine  
100 activation from  $\text{N}_2\text{O}_5$  uptake had a significant effect on daytime photolysis chemistry in China (Xue et  
101 al., 2015; Li et al., 2016; Tham et al., 2016; T. Wang et al., 2016).

102 In this study, to quantify the contribution of  $\text{NO}_3$  and  $\text{N}_2\text{O}_5$  chemistry to the atmospheric oxidation  
103 capacity and the  $\text{NO}_x$  removal process in the outflow of urban Beijing, we report the measurement of  
104  $\text{N}_2\text{O}_5$ ,  $\text{ClNO}_2$ , and related species in the surface layer of a suburban site in Beijing and determine the  
105  $\text{N}_2\text{O}_5$  heterogeneous uptake coefficients and  $\text{ClNO}_2$  yields. The nighttime  $\text{NO}_3$  oxidation of biogenic  
106 VOCs and its impact on the ON formation in the  $\text{NO}_x$ -rich region were diagnosed. Finally, the  
107 nighttime  $\text{NO}_x$  removal via  $\text{NO}_3$  and  $\text{N}_2\text{O}_5$  chemistry was estimated and discussed.

## 108 **2. Method**

### 109 **2.1 The site**

110 Within the framework of a Sino-Sweden joint research project, “Photochemical Smog in China”, a  
111 summer field campaign was conducted in Beijing to enhance our understanding of the secondary  
112 chemistry via photochemical smog and the heterogeneous reactions (Hallquist et al., 2016). The data  
113 presented here were collected at a regional site, PKU-CP (Peking University Changping campus), from  
114 23 May to 5 June 2016. The measurement site is located in the northern rural area of Beijing,  
115 approximately 45 km from the city center; the closest road is approximately 1 km to the south, and  
116 there are no major industry in the surroundings (Figure. 1). The site is surrounded to the north, east

117 and west by mountains. The general feature of this site is that it captures air masses with strong  
118 influences from both urban and biogenic emissions. Instruments were set up on the fifth floor of the  
119 main building of the campus with inlets approximately 12 m above the ground. Time is given in this  
120 paper as CNST (Chinese National Standard Time = UTC+8 h). During the campaign, sunrise was at  
121 05:00 CNST and sunset was at 19:30 CNST.

## 122 **2.2 Instrument setup**

123 A comprehensive suite of trace gas compounds and aerosol properties was measured in the field study,  
124 and the details are listed in Table 1.  $\text{N}_2\text{O}_5$  was measured by a newly developed cavity enhanced  
125 absorption spectrometer (CEAS; H. C. Wang et al., 2017a). In the CEAS, ambient  $\text{N}_2\text{O}_5$  was thermally  
126 decomposed to  $\text{NO}_3$  in a perfluoroalkoxy alkanes (PFA) tube (length: 35 cm, I.D.: 4.35 mm) heated to  
127 120 °C and was then detected within a PFA resonator cavity; the cavity was heated to 80 °C to prevent  
128  $\text{NO}_3$  reacting back to  $\text{N}_2\text{O}_5$ . Ambient gas was sampled with a 1.5-m sampling line (I.D.: 4.35 mm) with  
129 a flow rate of 2.0 L  $\text{min}^{-1}$ .  $\text{NO}$  was injected for 20 seconds to destroy  $\text{NO}_3$  from  $\text{N}_2\text{O}_5$  thermal  
130 decomposition in a 5-minute cycle, and the corresponding measurements were then used as reference  
131 spectra. A Teflon polytetrafluoroethylene (PTFE) filter was used in the front of the sampling module  
132 to remove ambient aerosol particles. The filter was replaced with a fresh one every hour to avoid the  
133 decrease of  $\text{N}_2\text{O}_5$  transmission efficiency due to aerosol accumulation on the filter. The limit of  
134 detection (LOD) was 2.7 pptv ( $1\sigma$ ), and the measurement uncertainty was 19%.

135  $\text{ClNO}_2$  and  $\text{N}_2\text{O}_5$  were also detected using a Time of Flight Chemical Ionization Mass Spectrometer  
136 (ToF-CIMS) with the Filter Inlet for Gas and AEROsols (FIGAERO; Lopez-Hilfiker et al., 2014;  
137 Bannan et al., 2015). Briefly, the gas phase species were measured via a 2-m-long, 6-mm-outer-  
138 diameter PFA inlet while the particles were simultaneously collected on a Teflon filter via a separate  
139 2-m-long, 10-mm-outer-diameter copper tubing inlet; both had flow rates of 2 L  $\text{min}^{-1}$ . The gas phase  
140 was measured for 25 minutes at 1 Hz, and the FIGAERO instrument was then switched to place the  
141 filter in front of the ion molecule region; it was then heated incrementally to 200 °C to desorb all the  
142 mass from the filter to be measured in the gas phase, which resulted in high-resolution thermograms.  
143 Formic acid calibrations were performed daily using a permeation source maintained at 40 °C. Post-  
144 campaign laboratory calibrations of  $\text{N}_2\text{O}_5$  were first normalized to the campaign formic acid  
145 calibrations to account for any change in sensitivity (Le Breton et al., 2014). Then,  $\text{ClNO}_2$   
146 measurements were quantified by passing the  $\text{N}_2\text{O}_5$  over a wetted  $\text{NaCl}$  bed to produce  $\text{ClNO}_2$ . The  
147 decrease in  $\text{N}_2\text{O}_5$  from the reaction with  $\text{NaCl}$  was assumed to be equal to the concentration of  $\text{ClNO}_2$   
148 produced (i.e., 100% yield). The sensitivities of the CIMS to  $\text{N}_2\text{O}_5$  and  $\text{ClNO}_2$  were found to be 9.5  
149 and 1.2 ion counts per pptv  $\text{Hz}^{-1}$ , respectively, with errors of 23% and 25% for  $\text{ClNO}_2$  and  $\text{N}_2\text{O}_5$ ,  
150 respectively. The LOD for  $\text{ClNO}_2$  and  $\text{N}_2\text{O}_5$  were 16 and 8 pptv, respectively. An intercomparison of  
151  $\text{N}_2\text{O}_5$  measurements between the CEAS and FIGAERO-ToF-CIMS showed good agreement; a  
152 companion paper on chlorine photochemical activation during this campaign gives detailed  
153 intercomparison results of  $\text{N}_2\text{O}_5$  measured by the two different techniques (Le Breton et al., 2018).

154 Sub-micron aerosol composition ( $\text{PM}_{1.0}$ ), including nitrate, sulfate, chloride, ammonium and  
155 organic compounds, were measured by a High Resolution Time of Flight Aerosol Mass Spectrometer  
156 (HR-ToF-AMS) (De Carlo et al, 2006, Zheng et al., 2017). Particle number and size distribution  
157 (PNSD) was measured by a scanning mobility particle sizer (SMPS, TSI 3936) and an aerosol particle

158 sizer (APS, TSI 3321) (Yue et al., 2009). SMPS measured the particles in the range between 3.5 nm  
159 and 523.3 nm in diameter, and APS measured the particles with a diameter range from 597.6 nm to  
160 10.0  $\mu\text{m}$ .  $S_a$  was calculated based on the dry-state particle number and geometric diameter in each size  
161 bin (3.5 nm - 2.5  $\mu\text{m}$ ). Dry-state  $S_a$  was corrected to wet particle-state  $S_a$  for particle hygroscopicity by  
162 a growth factor. The growth factor,  $f(\text{RH})=1 + 8.77 \times (\text{RH}/100)^{9.74}$ , was derived from the measurement  
163 of aerosol extinction as a function of RH in autumn in Beijing and is valid for  $30\% < \text{RH} < 90\%$  (Liu  
164 et al., 2013). The uncertainty of the wet aerosol surface areas was estimated to be  $\sim 30\%$ , associated  
165 from the error from dry PNSD measurement ( $\sim 20\%$ ) and the growth factor ( $\sim 20\%$ ). During this  
166 measurement, fine particles below 500 nm contributed to more than 90% of the total  $S_a$ .

167 VOCs were measured by Proton Transfer Reaction Mass Spectrometry (PTR-MS) with a time  
168 resolution of 5 minutes (de Gouw and Warneke et al., 2007; Wang et al., 2014). A commercial  
169 instrument (Thermo Electron model 42i) equipped with a molybdenum-catalytic converter was used  
170 to monitor  $\text{NO}_x$ . The LODs were 60 pptv (1 min) for NO and 300 pptv (1 min) for  $\text{NO}_2$ , with both at a  
171 20% precision (Tan et al., 2017). The molybdenum-catalytic technique not only converts  $\text{NO}_2$  to NO  
172 but also converts ambient  $\text{NO}_y$  such as peroxyacetyl nitrate (PAN) and  $\text{HNO}_3$ . Therefore, the measured  
173  $\text{NO}_2$  concentration corresponded to  $\text{NO}_2 + \text{NO}_y$  and was normally higher than the real concentration,  
174 especially in an aged air mass with high  $\text{NO}_x$  conditions. In this study, we used a factor of 0.6 to correct  
175 the nighttime  $\text{NO}_2$  concentration (a detailed explanation is in the Support Information Text S1 and  
176 Figure S1). The correction factor (0.6) is the average of the correction factors during nighttime. The  
177 standard deviation of the daytime correction factor for all the air masses experienced at Changping site  
178 was determined to be 0.27 ( $1\sigma$ ). If this uncertainty is extended to the nighttime correction factor, the  
179 resulting uncertainty of the nighttime correction is 45%. The uncertainty of  $\text{NO}_2$  is 50% when further  
180 included the associated measurement uncertainty from calibrations.  $\text{O}_3$  was measured by a commercial  
181 instrument using ultraviolet (UV) absorption (Thermo Electron model 49i); the LOD was 0.5 ppbv,  
182 with an uncertainty of 5%. The mass concentration of  $\text{PM}_{2.5}$  was measured using a standard Tapered  
183 Element Oscillating Microbalance (TEOM, 1400A analyzer). Meteorological parameters included  
184 relative humidity, temperature, pressure, wind speed, and wind direction and were available during the  
185 campaign. Photolysis frequencies were calculated from the spectral actinic photon flux density  
186 measured by a spectroradiometer (Bohn et al., 2008).

## 187 **3. Results**

### 188 **3.1 Overview**

189 During the campaign, the meteorological conditions of the site was high temperature and low relative  
190 humidity (RH); the temperature ranged from 10 - 34  $^\circ\text{C}$  and was  $23 \pm 5$   $^\circ\text{C}$  on average, and RH ranged  
191 from 10% - 80%, with an average of  $37\% \pm 15\%$ . Because of the special terrain of the observation site,  
192 the local wind was measured by the in situ meteorological stations; the site has a typical mountain-  
193 valley breeze that cannot reflect the general air mass movement patterns at slightly higher altitudes.  
194 Figure S2 shows the calculated backward trajectories using the Hybrid Single-Particle Lagrangian  
195 Integrated Trajectory (HYSPLIT) model (Draxler and Rolph, 2003). These images show the 24-h  
196 backward particle dispersion trajectories for 12:00 local time (CNST) as the starting time during May  
197 23 - July 5, 2016. The arrivals of air masses were mainly from the northwest and the south. Therefore,

198 we meteorologically separated the measurement period into two parts. The first three days show that  
199 the air masses came from the north or northwest; the air masses represent the background region  
200 (defined as Background Air Mass, BAM). The air masses after May 26 originated from the polluted  
201 NCP and passed over urban Beijing; they were characterized by large  $\text{NO}_x$  emissions and severe  
202 photochemical pollution (defined as Urban Air Mass, UAM).

203 The time series of  $\text{N}_2\text{O}_5$ ,  $\text{ClNO}_2$  and other relevant species are shown in Figure 2, and nighttime  
204 statistical results are listed in Table S1. The daily 8-h maximum of  $\text{O}_3$  concentration exceeded 93 ppbv  
205 (Chinese national air quality standard) for 8 of 12 days, and all the  $\text{O}_3$ -polluted air masses came from  
206 the urban region. When the air masses were from the background region, the daily maximum of  $\text{O}_3$   
207 was only approximately 60 ppbv, much lower than that from the urban region. The  $\text{NO}_2$  concentration  
208 was elevated, with a nocturnal average value over 10 ppbv during the urban air mass period. The  
209 nocturnal nitrate radical production rate,  $\text{P}(\text{NO}_3)$ , was large, with an average of  $1.2 \pm 0.9 \text{ ppbv h}^{-1}$ ,  
210 which is comparable with rates previously reported in the NCP and Hong Kong (Tham et al., 2016;  
211 Brown et al., 2016; Z. Wang et al., 2017; X. F. Wang et al., 2017). The daily peaks of  $\text{N}_2\text{O}_5$  were 100-  
212 500 pptv most nights; the maximum of 937 pptv in a 1-min average was observed near 20:00 on the  
213 early night of June 2, when the  $\text{P}(\text{NO}_3)$  was up to  $4 \text{ ppbv h}^{-1}$ . The average mixing ratio of  $\text{N}_2\text{O}_5$  was  $73$   
214  $\pm 90$  pptv, which is much higher than recent measurements reported in North China (Tham et al., 2016;  
215 X. F. Wang et al., 2017; Z. Wang et al., 2017), but much lower than that observed in the residual layer  
216 of the outflow from the PRD region, where the  $\text{N}_2\text{O}_5$  was up to 7.7 ppbv (T. Wang et al., 2016). With  
217 an elevated  $\text{O}_3$  mixing ratio in the first half of the night, the NO lifetime was only several minutes, and  
218 the mixing ratio of NO concentration was observed below the detection limit. During the second half  
219 of the night when the  $\text{O}_3$  concentration was consumed to low concentration, high levels of NO could  
220 occasionally be observed, and  $\text{N}_2\text{O}_5$  dropped to zero because of the fast titration by NO, such as the  
221 events that occurred on the second half of the nights of May 24, 28, 30. The  $\text{PM}_{2.5}$  mass concentration  
222 was moderate during the measurement period, with an average of  $26 \pm 21 \mu\text{g m}^{-3}$ , and the average  $S_a$   
223 was  $560 \pm 340 \mu\text{m}^2 \text{ cm}^{-3}$ . Elevated  $\text{ClNO}_2$  was observed with a daily maximum over 800 pptv (1-min  
224 average) during the urban air masses period. The maximum of  $\text{ClNO}_2$  was observed with 2900 pptv  
225 on the morning (05:30) of May 31. The observed  $\text{ClNO}_2$  in Beijing was comparable with those reported  
226 in NCP (Tham et al., 2016; X. Wang et al., 2017; Z. Wang et al., 2017), but slightly higher than that  
227 measured in coastal (e.g., Osthoff et al., 2008) and inland sites (e.g., Thornton et al., 2010). Overall,  
228 high  $\text{ClNO}_2$  observed in this site suggested fast  $\text{N}_2\text{O}_5$  heterogeneous hydrolysis and effective  $\text{ClNO}_2$   
229 yields are common in Beijing.

### 230 3. 2 Mean diurnal profiles

231 The mean diurnal profiles of the measured  $\text{NO}_2$ ,  $\text{O}_3$ ,  $\text{N}_2\text{O}_5$ ,  $\text{ClNO}_2$  and the particle chloride content are  
232 shown in Figure 3, as well as the calculated  $\text{NO}_3$  based on the thermal equilibrium of  $\text{NO}_2$ ,  $\text{NO}_3$  and  
233  $\text{N}_2\text{O}_5$ . The left panel show the average results of the BAM period, and the right panels show those of  
234 the UAM period.  $\text{NO}_2$  and  $\text{O}_3$  from the UAM were much higher than those from the BAM, as well as  
235 the mixing ratios of  $\text{N}_2\text{O}_5$ ,  $\text{NO}_3$  and  $\text{ClNO}_2$ , but the daily variation tendencies of those species in the  
236 two kinds of air masses were similar.  $\text{N}_2\text{O}_5$  began to accumulate in the late afternoon and increased  
237 sharply after sunset. A peak occurred near 20:00 and decreased below the instrument detection limit at  
238 sunrise. The time that  $\text{N}_2\text{O}_5$  maxima occurred is similar to our previous observation in urban Beijing

239 (H. C. Wang et al., 2017c). However, the decrease rate of the observed N<sub>2</sub>O<sub>5</sub> after the peak time was  
 240 much slower than that in urban Beijing, where the N<sub>2</sub>O<sub>5</sub> dropped to zero in 2-4 hours, which suggests  
 241 a relatively slow N<sub>2</sub>O<sub>5</sub> loss rate in suburban Beijing. The daily average peaks of N<sub>2</sub>O<sub>5</sub> during the BAM  
 242 period and the UAM period were 75 pptv and 150 pptv, respectively. The calculated NO<sub>3</sub> diurnal  
 243 profile was quite similar to N<sub>2</sub>O<sub>5</sub>, and the daily average peaks of NO<sub>3</sub> during the BAM and UAM  
 244 periods were approximately 11 pptv and 27 pptv, respectively. The uncertainty of NO<sub>3</sub> calculation was  
 245 estimated to be 67% according to Eq. 2, which is dominated by the uncertainty of NO<sub>2</sub> measurement.

$$246 \frac{\Delta[\text{NO}_3]}{[\text{NO}_3]} = \sqrt{\left(\frac{\Delta[\text{N}_2\text{O}_5]}{[\text{N}_2\text{O}_5]}\right)^2 + \left(\frac{\Delta[\text{NO}_2]}{[\text{NO}_2]}\right)^2 + \left(\frac{\Delta[\text{O}_3]}{[\text{O}_3]}\right)^2 + \left(\frac{\Delta K_{\text{eq}}}{K_{\text{eq}}}\right)^2} \quad (\text{Eq. 2})$$

247 The observed ClNO<sub>2</sub> concentrations showed a clear increase after sunset, ClNO<sub>2</sub> reached a  
 248 maximum before sunrise for BAM period but around midnight for the UAM period. The diurnal peak  
 249 of ClNO<sub>2</sub> in the BAM period was 125 pptv, whereas the diurnal peak of ClNO<sub>2</sub> was over 780 pptv in  
 250 the UAM period, and 6 times as high as that in the UAM period. Particulate chloride (Cl<sup>-</sup>) is a key  
 251 factor that affects the ClNO<sub>2</sub> yield on aerosol surface. Higher particle chloride leads to higher ClNO<sub>2</sub>  
 252 yield and promotes the N<sub>2</sub>O<sub>5</sub> conversion to ClNO<sub>2</sub> (e.g., Finlayson-Pitts et al., 1989; Behnke et al.,  
 253 1997), whereas the particle chloride content during the measurement was below 60 pptv and was much  
 254 lower than the mixing ratio of ClNO<sub>2</sub>, suggest a nighttime continuously Cl source replenished to  
 255 support the ClNO<sub>2</sub> formation. The HYSPLIT showed that the air masses mainly came from continental,  
 256 not from the coastal regime, suggested that large amounts of the Cl<sup>-</sup> were not replenished by NaCl  
 257 from marine sources, but possibly replenished by gas-phase HCl through the acid displacement  
 258 reaction (Ye et al., 2016). Cl<sup>-</sup> was found to be correlated strongly with CO and SO<sub>2</sub>, likely to originate  
 259 from an anthropogenic source, such as power plants or combustion sources (Le Breton et al., 2018).  
 260 According to the mass balance, the gas phase HCl for supporting the production of ClNO<sub>2</sub> is several  
 261 ppbv per night. The required HCl source indicated the ratio HCl/pCl<sup>-</sup> is about 10-30, which was found  
 262 consistent with the following observation in Beijing. Although the HCl measurement was not available  
 263 in this study, note that up to 10 ppbv of HCl was observed in the urban Beijing in September, 2016,  
 264 we purpose that the gas phase HCl was sufficient to support the ClNO<sub>2</sub> formation.

265 After sunrise, ClNO<sub>2</sub> was photolyzed and decreased with the increasing photolysis intensity;  
 266 However, the ClNO<sub>2</sub> can still survive until noon with the averaged daily maximum of  $J(\text{ClNO}_2)$  to be  
 267  $1.7 \times 10^{-4} \text{ s}^{-1}$ . Similar to the studies reported in London, Texas and Wangdu (Bannan et al., 2015; Faxon  
 268 et al., 2015; Tham et al., 2016), we observed sustained elevated ClNO<sub>2</sub> events after sunrise in 5 of 12  
 269 days. For example, on the morning of May 30, ClNO<sub>2</sub> increased fast after sunrise and up to 500 pptv  
 270 at 8:00 am. Such high ClNO<sub>2</sub> increasing was impossible attribute to the local chemical formation since  
 271 N<sub>2</sub>O<sub>5</sub> dropped to almost zero and the needed N<sub>2</sub>O<sub>5</sub> uptake coefficients were unrealistically high.  
 272 Previous study suggested that abundant ClNO<sub>2</sub> produced in the residual layer at night and downward  
 273 transport in the morning may help to explain this phenomenon (Tham et al., 2016).

### 274 3.3 Variation of N<sub>2</sub>O<sub>5</sub> in the background air masses

275 During the BAM period, the O<sub>3</sub> concentration was well in excess of NO<sub>2</sub>. In the NO<sub>3</sub> and N<sub>2</sub>O<sub>5</sub>  
276 formation processes, the limited NO<sub>2</sub> in high O<sub>3</sub> region indicates that the variation of NO<sub>2</sub> is more  
277 essential to the variation of the N<sub>2</sub>O<sub>5</sub> concentration. As shown in Figure 4, during the night of May 24  
278 (20:00 - 04:00), the local emission of NO was negligible. O<sub>3</sub> concentration was larger than 25 ppbv,  
279 much higher than NO<sub>2</sub> and free of the local NO emission. The N<sub>2</sub>O<sub>5</sub> concentration was highly  
280 correlated with NO<sub>2</sub> ( $R^2 = 0.81$ ) and the NO<sub>3</sub> production rate ( $R^2 = 0.60$ ), suggests the N<sub>2</sub>O<sub>5</sub>  
281 concentration was solely response to the NO<sub>2</sub> concentration in the background air mass when enough  
282 O<sub>3</sub> is presented.

### 283 3.4 Elevated ClNO<sub>2</sub> to N<sub>2</sub>O<sub>5</sub> ratio

284 Large day-to-day variabilities of N<sub>2</sub>O<sub>5</sub> and ClNO<sub>2</sub> were observed during the measurement period.  
285 Following the work of Osthoff et al. (2008), Mielke et al. (2013), Phillips et al. (2012) and Bannan et  
286 al. (2015), we used the concentration ratio of ClNO<sub>2</sub> to N<sub>2</sub>O<sub>5</sub>, to describe the conversion capacity of  
287 N<sub>2</sub>O<sub>5</sub> to ClNO<sub>2</sub>. Although N<sub>2</sub>O<sub>5</sub> is lost to dry deposition in near surface measurements and would drive  
288 up the ClNO<sub>2</sub>:N<sub>2</sub>O<sub>5</sub>. The nighttime peak values and mean values of ClNO<sub>2</sub>: N<sub>2</sub>O<sub>5</sub> were used to calculate  
289 the daily ratios (Table S2), the calculation period is from 19:30 to the next day 05:00. The average  
290 nighttime ratio ranged from 0.7 to 42.0, with a mean of 7.7 and a median of 6.0. The ClNO<sub>2</sub> formation  
291 was effective, with ClNO<sub>2</sub>:N<sub>2</sub>O<sub>5</sub> ratios larger than 1:1 throughout the campaign, except for the night  
292 of May 26, when the ratio was 0.7:1. Previous observations of the ClNO<sub>2</sub>:N<sub>2</sub>O<sub>5</sub> ratios are summarized  
293 in Table 2. Compared with the results conducted in similar continental regions in Europe and America  
294 (0.2 - 3.0), the ratios in this work were significantly higher and consistent with the recent studies in  
295 the NCP (Tham et al., 2016; X. F. Wang et al., 2017; Z. Wang et al., 2017), which suggests that high  
296 ClNO<sub>2</sub>: N<sub>2</sub>O<sub>5</sub> ratios were ubiquitous in the NCP and implies that the ClNO<sub>2</sub> yield via N<sub>2</sub>O<sub>5</sub> uptake is  
297 efficient.

## 298 4. Discussion

### 299 4.1 Determination of N<sub>2</sub>O<sub>5</sub> uptake coefficients

300 A composite term,  $\gamma \times f$ , was used to evaluate the production of ClNO<sub>2</sub> from N<sub>2</sub>O<sub>5</sub> heterogeneous  
301 hydrolysis (Mielke et al., 2013).  $\gamma \times f$  was estimated by fitting the observed ClNO<sub>2</sub> in a time period  
302 when the nighttime concentrations of ClNO<sub>2</sub> increased continuously at night. The increased ClNO<sub>2</sub>  
303 was assumed to be solely from the N<sub>2</sub>O<sub>5</sub> uptake. The fitting was optimized by changing the input of  $\gamma$   
304  $\times f$  associated with the measured N<sub>2</sub>O<sub>5</sub> and  $S_a$ , until the ClNO<sub>2</sub> increasing was well reproduced (Eq. 3).

$$305 \quad [\text{ClNO}_2](t) = [\text{ClNO}_2](t_0) + (\gamma \times f) \cdot \int_{t_0}^t \frac{C \cdot S_a}{4} [\text{N}_2\text{O}_5] dt \quad (\text{Eq. 3})$$

306 Here  $t_0$  and  $t$  denote the start time and end time, respectively, the calculation time duration was  
307 normally several hours.  $[\text{ClNO}_2](t_0)$  is the observed concentration at  $t_0$  and set as the fitting offset. Note  
308 that the transport leads to the bias of N<sub>2</sub>O<sub>5</sub> uptake coefficient and ClNO<sub>2</sub> yield. But the small variation  
309 of the mixing ratio of CO (< 5%) during each analysis time periods suggested the transport process is



310 not important to the increasing ClNO<sub>2</sub>. The derived  $\gamma \times f$  was found to be constant with small  
311 uncertainties for optimization (see Table S3). The  $\gamma \times f$  had moderate variability, ranged from 0.008 -  
312 0.035 with an average of  $0.019 \pm 0.009$ . Table 3 summarizes the  $\gamma \times f$  values derived in the previous  
313 field observations. The value in suburban Germany was between 0.001 and 0.09, with the average of  
314 0.014 (Phillips et al., 2016), and the average value in Mt. Tai, China, was approximately 0.016 (Z.  
315 Wang et al., 2017). The average  $\gamma \times f$  in this study was comparable with that of the two suburban sites,  
316 whereas in an urban site of Jinan, China (X. F. Wang et al., 2017), the value was lower than 0.008 and  
317 comparable with that in the CalNex-LA campaign. The three sets of  $\gamma \times f$  values from suburban regions  
318 were about twice as large as those in urban regions, which implies that the ClNO<sub>2</sub> formation efficiency  
319 in the aged air masses in suburban regions were more efficient than in the urban region. The difference  
320 of the overall yield between the two regions may be caused by particle properties or other factors  
321 (Riemer et al., 2009; Gaston et al., 2014; Grzanic et al., 2015; Bertram and Thornton, 2009).

322 According to reaction R4, soluble nitrate and ClNO<sub>2</sub> were formed by N<sub>2</sub>O<sub>5</sub> heterogeneous uptake,  
323 with yields of  $2 - f$  and  $f$ , respectively. Following the recent work of Phillips et al., (2016), we used the  
324 observed pNO<sub>3</sub><sup>-</sup> and ClNO<sub>2</sub> formation rates to derive individual  $\gamma$  and  $f$ . The calculations assumed that  
325 the relevant properties of the air mass are conserved and that the losses of produced species are  
326 negligible; additionally, the N<sub>2</sub>O<sub>5</sub> uptake coefficients and the ClNO<sub>2</sub> yield are independent of particle  
327 size. The nights characterized by the following two features were chosen for further analysis: (1)  
328 significant correlations between pNO<sub>3</sub><sup>-</sup> and ClNO<sub>2</sub> were present ( $R^2 > 0.5$ ), which suggested that, to a  
329 good approximation, both ClNO<sub>2</sub> and pNO<sub>3</sub><sup>-</sup> are produced only by N<sub>2</sub>O<sub>5</sub> heterogeneous uptake. The  
330 reason for excluding other nights with low correction ( $R^2 < 0.2$ ) was ClNO<sub>2</sub> and pNO<sub>3</sub><sup>-</sup> may be affected  
331 by the effective transport or other production pathways, and these contributions can't be well quantified.  
332 Therefore the selection of high correction of ClNO<sub>2</sub> with pNO<sub>3</sub><sup>-</sup> may be lead a bias as the contribution  
333 from other formation pathways and the transport were neglected. (2) During an increasing period of  
334 pNO<sub>3</sub><sup>-</sup>, an equivalent or faster increase of ammonium molar ratio to pNO<sub>3</sub><sup>-</sup> was also observed, which  
335 means enough gas-phase ammonia was repartitioned to form ammonium nitrate and suppress the  
336 release of HNO<sub>3</sub>. The ammonia rich conditions ( $22 \pm 9$  ppbv on average) in Beijing demonstrated that  
337 the degassing of HNO<sub>3</sub> at night can be effectively buffered by the high concentrations of ammonia  
338 presented in the NCP (Liu et al., 2017). Both the gas-particle repartitioning of HNO<sub>3</sub> or nighttime  
339 produced HNO<sub>3</sub> will result in the overestimation of  $\gamma$  and the underestimation of  $f$ . The daytime  
340 produced HNO<sub>3</sub> will be soon in a new equilibrium rapidly on the time scale of total nitrate chemical  
341 production, and the nighttime formation of HNO<sub>3</sub> are normally not important, so the nocturnal HNO<sub>3</sub>  
342 uptake impact is negligible. During this campaign, five nights were eligible for the following analysis.  
343 Based on the observational data of N<sub>2</sub>O<sub>5</sub>, ClNO<sub>2</sub>, pNO<sub>3</sub><sup>-</sup> and  $S_a$  in 5 minutes average. The formations  
344 of pNO<sub>3</sub><sup>-</sup> and ClNO<sub>2</sub> were integrated to reproduce the increasing pNO<sub>3</sub><sup>-</sup> and ClNO<sub>2</sub> by input an initial  
345  $\gamma$  and  $f$ . The offset of pNO<sub>3</sub><sup>-</sup> and ClNO<sub>2</sub> is the measured pNO<sub>3</sub><sup>-</sup> and ClNO<sub>2</sub> concentration at the start  
346 time. The  $\gamma$  and  $f$  were optimized based on the Levenberg-Marquardt algorithm until good agreement  
347 between the observed and predicted concentrations of pNO<sub>3</sub><sup>-</sup> and ClNO<sub>2</sub> was obtained (Phillips et al.,  
348 2016). Figure 5 depicts an example of the fitting results on May 28. The predicted N<sub>2</sub>O<sub>5</sub> uptake  
349 coefficient and ClNO<sub>2</sub> yield were 0.017 and 1.0, respectively. The uncertainty on each individual fitting  
350 is varied from 55% - 100% due to the variability and measurements uncertainties of pNO<sub>3</sub><sup>-</sup> and ClNO<sub>2</sub>.  
351 Five sets of values of  $\gamma$  and  $f$  obtained are listed in Table 4. N<sub>2</sub>O<sub>5</sub> uptake coefficients ranged from 0.012  
352 - 0.055, with an average of  $0.034 \pm 0.018$ , and the ClNO<sub>2</sub> yield ranged from 0.50 to unity, with an

353 average of  $0.73 \pm 0.25$ . The errors from each derivation were 55% and came from the field  
354 measurements of  $S_a$ ,  $N_2O_5$ ,  $pNO_3^-$  and  $ClNO_2$ .

355 The average  $\gamma$  value was consistent with the results determined by the same method in a rural site in  
356 Germany (Phillips et al., 2016), but was higher than those in the UK and North America where they  
357 used other derivation methods, included the steady state lifetime method (Morgan et al., 2015; Brown  
358 et al., 2006, 2009), the iterated box model (Wagner et al., 2013) and direct measurement based on an  
359 aerosol flow reactor (Bertram et al., 2009; Riedel et al., 2012). The steady state lifetime method is very  
360 sensitive to  $NO_2$  concentration, and since the  $NO_2$  measurement suffered with ambient  $NO_y$   
361 interference, we did not apply the steady state lifetime method in this study (Brown et al., 2003).  
362 Nonetheless, the derived  $\gamma$  in Beijing showed good agreement with the recent results derived by the  
363 steady state method in Jinan and Mt. Tai (X. F. Wang et al., 2017; Z. Wang et al., 2017). The  
364 consistency eliminates the discrepancy possibly brought by the differences of analysis methods.  
365 Therefore, we suggest that fast  $N_2O_5$  uptake was a ubiquitous feature that existed in the NCP. In this  
366 study, sulfate is the dominant component of  $PM_{1.0}$ , accounting for more than 30% of its mass  
367 concentration, which may be the reason of elevated  $N_2O_5$  uptake coefficient presented in Beijing, like  
368 the result in high sulfate air mass over Ohio and western Pennsylvania (Brown et al., 2006). Previous  
369 studies have shown that the  $N_2O_5$  uptake coefficient strongly depends on the liquid water content, the  
370  $pNO_3^-$  and organic mass. Liquid water content promotes  $N_2O_5$  uptake, whereas  $pNO_3^-$  and organic  
371 mass inhibit  $N_2O_5$  uptake (e.g., Thornton et al., 2003, Wahner et al., 1998; Bertram and Thornton,  
372 2009). Because of the limited data set of  $N_2O_5$  uptake coefficients in this work, the function  
373 dependence studies about the determined  $N_2O_5$  uptake coefficients with the parameters mentioned  
374 above were not convincing. More valid data are needed in the further studies of the  $N_2O_5$  uptake  
375 mechanism. With respect to  $f$ , the values are comparable with that observed in Germany (Phillips et  
376 al., 2016) and are similar to that estimated in the power plant plume in Mt. Tai with high chloride  
377 content (Z. Wang et al., 2017).

## 378 4.2 $N_2O_5$ lifetime and reactivity

379 The lifetime of  $N_2O_5$  was estimated by the steady state method, assuming that the production and loss  
380 of  $N_2O_5$  was in balance after a period following sunset. Eq. 4 for the steady state approximation has  
381 been frequently applied in analyzing the fate of  $N_2O_5$  (Platt et al., 1980; Allan et al., 1999; Brown et  
382 al., 2003).

$$383 \quad \tau_{ss}(N_2O_5) = \frac{1}{L_{ss}(N_2O_5)} = \frac{[N_2O_5]}{k_{NO_2+O_3}[NO_2][O_3]} \quad (\text{Eq. 4})$$

384 Here  $\tau_{ss}(N_2O_5)$  denotes the steady state lifetime of  $N_2O_5$  and  $L_{ss}(N_2O_5)$  denotes the loss term of  $N_2O_5$   
385 corresponding to the steady state lifetime. A numerical model was used to check the validity of the  
386 steady state approximation (Brown et al., 2003); details are given in Figure S3. The results show that  
387 the steady state can generally be achieved within 30 minutes. In this study, the steady state lifetime  
388 was only calculated from 20:00 to the next day 04:00. The time periods with  $NO$  concentration larger  
389 than 0.06 ppbv (instrument LOD) were excluded as the steady state is easily disturbed. The overall  
390  $N_2O_5$  loss rate ( $k(N_2O_5)$ ) can be calculated by accumulating each individual loss term in Eq. 5,  
391 including the  $N_2O_5$  heterogeneous hydrolysis and the reaction of  $NO_3$  with VOCs.

$$k(\text{N}_2\text{O}_5) = \frac{\sum k_{\text{NO}_3+\text{VOC}_i} \cdot [\text{VOC}_i]}{k_{\text{eq}} \cdot [\text{NO}_2]} + \frac{C \cdot S_a \cdot \gamma}{4} \quad (\text{Eq. 5})$$

393 The  $\text{NO}_3$  heterogeneous uptake and the loss of  $\text{N}_2\text{O}_5$  via gas-phase reactions were assumed to be  
 394 negligible (Brown and Stutz, 2012).  $k_{\text{NO}_3+\text{VOC}_i}$  denotes the reaction rate constants of the reaction of  
 395  $\text{NO}_3+\text{VOC}_i$ . Isoprene and monoterpene were used in this calculation.

396 The  $\text{N}_2\text{O}_5$  loss rate coefficient by heterogeneous hydrolysis was calculated by using an average  $\gamma$  of  
 397 0.034. The time series of the steady state lifetime of  $\text{N}_2\text{O}_5$  is shown in Figure S4. The  $\text{N}_2\text{O}_5$  steady state  
 398 lifetime ranged from  $<5$  s to 1260 s, with an average of  $270 \pm 240$  s, and large variability was shown  
 399 during the campaign. The  $\text{N}_2\text{O}_5$  lifetimes during the BAM period were higher than those during the  
 400 UAM period, which is predictable since the clean air mass has lower  $\text{N}_2\text{O}_5$  reactivity because of much  
 401 lower aerosol loading. Two extremely short  $\text{N}_2\text{O}_5$  lifetime cases were captured on the nights of May  
 402 30 and June 3, with peak values below 200 s throughout those nights. Figure 6 shows that the  $\text{N}_2\text{O}_5$   
 403 lifetime had a very clear negative dependence on the ambient  $S_a$  when larger than  $300 \mu\text{m}^2 \text{cm}^{-3}$ , which  
 404 indicates that the  $\text{N}_2\text{O}_5$  heterogeneous uptake plays an important role in the regulation of  $\text{N}_2\text{O}_5$  lifetime.  
 405 The study conducted in the residual layer of Hong Kong showed a similar tendency despite the overall  
 406  $\text{N}_2\text{O}_5$  lifetime being shorter at this site (Brown et al., 2016). Additionally, a negative dependence of  
 407  $\text{N}_2\text{O}_5$  lifetime on RH was reported in Hong Kong but was not observed in this study (Figure S5).

408 Figure 7 shows the time series of the overall  $\text{N}_2\text{O}_5$  loss rate constant as well as the  $\text{N}_2\text{O}_5$  steady state  
 409 loss rate constant. The overall  $\text{N}_2\text{O}_5$  loss rate constant was calculated from the individual terms (Eq.3).  
 410 The uncertainties of the  $\text{N}_2\text{O}_5$  steady state loss rate constant and the overall  $k(\text{N}_2\text{O}_5)$  are estimated to  
 411 be 67% and 95%, respectively (Eq. 6 and Eq. 7). The largest error sources were from the corrected  
 412  $\text{NO}_2$  measurements.

$$413 \frac{\Delta L_{SS}(\text{N}_2\text{O}_5)}{L_{SS}(\text{N}_2\text{O}_5)} = \sqrt{\left(\frac{\Delta[\text{N}_2\text{O}_5]}{[\text{N}_2\text{O}_5]}\right)^2 + \left(\frac{\Delta[\text{NO}_2]}{[\text{NO}_2]}\right)^2 + \left(\frac{\Delta[\text{O}_3]}{[\text{O}_3]}\right)^2 + \left(\frac{\Delta K_{\text{eq}}}{K_{\text{eq}}}\right)^2} \quad (\text{Eq. 6})$$

$$414 \frac{\Delta k(\text{N}_2\text{O}_5)}{k(\text{N}_2\text{O}_5)} = \sqrt{\left(\frac{\Delta[\text{N}_2\text{O}_5]}{[\text{N}_2\text{O}_5]}\right)^2 + \left(\frac{\Delta[S_a]}{[S_a]}\right)^2 + \left(\frac{\Delta[\gamma]}{[\gamma]}\right)^2 + \left(\frac{\Delta[\text{NO}_2]}{[\text{NO}_2]}\right)^2 + \left(\frac{\Delta[\text{O}_3]}{[\text{O}_3]}\right)^2 + \left(\frac{\Delta[\text{VOC}_i]}{[\text{VOC}_i]}\right)^2 + \left(\frac{\Delta K_{\text{eq}}}{K_{\text{eq}}}\right)^2} \quad (\text{Eq. 7})$$

415 On the night of 29 May, the steady state loss rate constant was much lower than the overall  $k(\text{N}_2\text{O}_5)$ ;  
 416 on the nights of 28, May and 3 June, the  $L_{SS}(\text{N}_2\text{O}_5)$  calculated by the steady state method were much  
 417 higher than the overall  $k(\text{N}_2\text{O}_5)$ , but these discrepancies were in the range of the uncertainties. The  
 418 steady state loss rate constant in the case of May 30 was approximately ten times larger than the overall  
 419 loss rate constant, and this difference was outside of the range of uncertainty. The reason for the larger  
 420 difference on this night is not understood from the available measurements. In general, the overall  
 421  $\text{N}_2\text{O}_5$  loss rate constant and the steady state  $\text{N}_2\text{O}_5$  loss rate constant were comparable taking into  
 422 considerations of the uncertainties. The average  $\text{N}_2\text{O}_5$  loss rate constant contributed by the  $\text{N}_2\text{O}_5$   
 423 heterogeneous hydrolysis was  $8.1 \times 10^{-4} \text{ s}^{-1}$ . The average  $\text{NO}_3$  loss rate constant by the reaction of  $\text{NO}_3$   
 424 with VOCs was  $0.015 \pm 0.007 \text{ s}^{-1}$ , which is comparable with the previous results in suburban Beijing  
 425 in 2006 (H. C. Wang et al., 2017c), in which the contribution to the  $\text{N}_2\text{O}_5$  reactivity was  $1.63 \times 10^{-3} \pm$   
 426  $0.65 \times 10^{-3} \text{ s}^{-1}$  on average. Compared with  $\text{N}_2\text{O}_5$  loss via direct heterogeneous hydrolysis, the indirect  
 427 loss via  $\text{NO}_3+\text{VOC}_i$  was dominant, accounting for approximately 67%. Because only a subset of the

428 suite of organic species at the site was measured, the calculated loss rate constant via  $\text{NO}_3+\text{VOCs}$   
429 represents a lower limit. Therefore, the  $\text{N}_2\text{O}_5$  loss via  $\text{NO}_3+\text{VOCs}$  may occupy a larger proportion. The  
430 overall loss rate constant from  $\text{NO}_3+\text{VOCs}$  and  $\text{N}_2\text{O}_5$  uptake was  $2.44\times 10^{-3} \pm 1.5\times 10^{-3} \text{ s}^{-1}$  on average,  
431 which was reasonably lower than the steady state  $\text{N}_2\text{O}_5$  loss rate constant of  $3.61\times 10^{-3} \pm 2.80\times 10^{-3} \text{ s}^{-1}$   
432 on average. The gap may be explained by the unmeasured reactive VOCs or the unaccounted NO that  
433 was near the instrumental limit of detection.

### 434 4.3 $\text{NO}_3$ -induced nocturnal oxidation of VOCs

435 Recent studies have suggested that the fate of BVOCs after sunset is dominated by  $\text{NO}_x$  or  $\text{O}_3$ , with  
436 variation of the ratio of  $\text{NO}_x$  to BVOCs and that the nighttime oxidation is located in the transition  
437 region between  $\text{NO}_x$ -domination and  $\text{O}_3$ -domination in the United States (Edwards et al., 2017).  
438 During this campaign, the nocturnal average concentrations of isoprene and monoterpene were  $156 \pm$   
439  $88 \text{ pptv}$  and  $86 \pm 42 \text{ pptv}$ , respectively. We used isoprene and monoterpene to represent a lower limit  
440 mixing ratio of total BVOCs; the average ratio of  $\text{NO}_x/\text{BVOCs}$  was larger than 10 and exhibited small  
441 variation during the BAM and UAM periods. The value was much higher than the critical value ( $\text{NO}_x$   
442  $/\text{BVOC} = 0.5$ ) of the transition regime proposed by Edwards et al. (2017), which suggests that the  
443 oxidation of BVOCs in Beijing was  $\text{NO}_x$ -dominated and the nighttime fate of BVOCs was controlled  
444 by  $\text{NO}_3$ . Since the reaction of  $\text{NO}_3$  with BVOCs has a high mass yield, the nocturnal ON production  
445 may be important in the high  $\text{NO}_x/\text{BVOCs}$  region.

446 The first order loss rate of VOCs initialized by oxidants,  $k(\text{VOCs}_i)$ , is defined as VOCs reactivity  
447 and expressed as Eq. 8. Here, we only consider the reaction of VOCs with  $\text{O}_3$  and  $\text{NO}_3$ .  $k_{\text{O}_3+\text{VOCs}_i}$   
448 denotes the reaction rate constants of  $\text{VOCs}_i$  with  $\text{O}_3$ .

$$449 \quad k(\text{VOCs}_i) = k_{\text{NO}_3+\text{VOCs}_i} \cdot [\text{NO}_3] + k_{\text{O}_3+\text{VOCs}_i} \cdot [\text{O}_3] \quad (\text{Eq. 8})$$

450 During this campaign, VOCs reactivity could be determined with the measured  $\text{O}_3$  and calculated  $\text{NO}_3$ .  
451 Figure 8 depicts four kinds of VOCs reactivity distribution during nighttime, including the isoprene  
452 (ISO), monoterpene (MNT), the double bond at the end or terminal position of the molecule (OLT)  
453 and alkenes with the double bond elsewhere in the molecule (OLI). The reaction rates were cited from  
454 the regional atmospheric chemistry mechanism version 2 (RACM2, Goliff et al., (2013)). Previous  
455 measurement indicated the main detectable monoterpenes were  $\alpha$ -pinene and  $\beta$ -pinene in summer  
456 Beijing (personal communication with Ying Liu). Here we assumed  $\alpha$ -pinene and  $\beta$ -pinene occupies  
457 half and half in the monoterpene with an uncertainty of 50%. The rate coefficients of  $\alpha$ -pinene and  $\beta$ -  
458 pinene with  $\text{NO}_3$  were referred to Atkinson and Arey, (2003). The uncertainty of calculated mixing  
459 ratio of  $\text{NO}_3$  is 67%, and the overall uncertainty of monoterpene reactivity was calculated to be 85%  
460 by Gaussian propagation. The uncertainties of other kinds of VOCs was calculated to be 75% by  
461 assuming the uncertainty of rate coefficient was 30%. The VOCs reactivity were dominated by  $\text{NO}_3$   
462 oxidation and contributed up to 90% in total; less than 10% VOCs were oxidized by  $\text{O}_3$  during the  
463 nighttime. Even the  $\text{NO}_3$  concentration in the lower range,  $\text{NO}_3$  still responsible for more than 70%  
464 nocturnal BVOCs oxidation, the results further confirmed that the oxidation of BVOCs is controlled  
465 by  $\text{NO}_3$  rather than  $\text{O}_3$  in summer Beijing.

466 For calculating nocturnal ON production from NO<sub>3</sub> oxidation of isoprene and monoterpene, as well  
467 as inorganic nitrate production via N<sub>2</sub>O<sub>5</sub> heterogeneous uptake over the same period, the ClNO<sub>2</sub> yield  
468 was set to the determined average value of 0.55. The organic nitrate yield of the reaction of NO<sub>3</sub> with  
469 isoprene was set to 0.7, from Rollins et al. (2009). The yield from the reaction of NO<sub>3</sub> with  
470 monoterpene was represented by NO<sub>3</sub> + $\alpha$ -pinene and was set to 0.16, following Spittler et al. (2006).  
471 As the  $\alpha$ -pinene and  $\beta$ -pinene have very different ON yields, the yield set in the study was an upper  
472 limit for  $\alpha$ -pinene initiated ON, but is relative low yield for the  $\beta$ -pinene initialized ON (e.g., Hallquist  
473 et al., 1999). Although the yield from the NO<sub>3</sub> oxidation of isoprene is much higher than that of  
474 monoterpene, the total ON production was dominated by the oxidation of NO<sub>3</sub> with monoterpene  
475 because the reaction of NO<sub>3</sub> with monoterpene is much faster than that with isoprene. Because of the  
476 lack of measurement of alkenes and other VOCs that can react with NO<sub>3</sub> and form ON, the calculated  
477 nighttime ON production rate analyzed here served as a lower estimations.

478 Figure 9 depicts the mean diurnal profiles of the nocturnal formation rates of inorganic nitrates and  
479 ON. The average production rate of ON was up to  $0.10 \pm 0.07$  ppbv h<sup>-1</sup>, which was higher than that  
480 predicted in a suburban site in Beijing in 2006, with an average value of  $0.06$  ppbv h<sup>-1</sup> (H.C. Wang et  
481 al., 2017b). In the high NO<sub>x</sub>/BVOCs air masses, the inorganic nitrate formation was proposed to  
482 increase with the increase of sunset NO<sub>x</sub>/BVOCs (Edwards et al., 2017). The formation rate of  
483 inorganic nitrate via N<sub>2</sub>O<sub>5</sub> uptake was significant, with an average of  $0.43 \pm 0.12$  ppbv h<sup>-1</sup>, and was  
484 much larger than the ON formation. NO<sub>x</sub> was mainly removed as the inorganic nitrate format by  
485 nocturnal NO<sub>3</sub>-N<sub>2</sub>O<sub>5</sub> chemistry in Beijing. Overall, the NO<sub>3</sub>-N<sub>2</sub>O<sub>5</sub> chemistry led to significant NO<sub>x</sub>  
486 removal, with  $0.54$  ppbv h<sup>-1</sup> accounted for by the organic and inorganic nitrates, and the integral NO<sub>x</sub>  
487 removal was approximately 5 ppbv per night. Since ON are important precursors of the secondary  
488 organic aerosols (SOA), the NO<sub>3</sub> oxidation was very important from the perspective of organic aerosol  
489 formation and regional particulate matter (e.g., Ng et al., 2008).

## 490 5. Conclusion

491 We reported an intensive field study of NO<sub>3</sub>-N<sub>2</sub>O<sub>5</sub> chemistry at a downwind suburban site in Beijing  
492 during the summer of 2016. High levels of ClNO<sub>2</sub> and N<sub>2</sub>O<sub>5</sub> were observed, with maxima of 2.9 ppbv  
493 and 937 pptv (1-min), respectively. The N<sub>2</sub>O<sub>5</sub> uptake coefficient was estimated to be in the range of  
494 0.010-0.055, with an average value of  $0.034 \pm 0.018$ , and the corresponding ClNO<sub>2</sub> yield was derived  
495 to be in the range of 0.5-1.0, with an average value of  $0.73 \pm 0.25$ . The elevated ClNO<sub>2</sub> levels and  
496 ClNO<sub>2</sub>/N<sub>2</sub>O<sub>5</sub> ratios are comparable with those in chloride-rich regions in the NCP. The results highlight  
497 fast N<sub>2</sub>O<sub>5</sub> heterogeneous hydrolysis and efficient ClNO<sub>2</sub> formation in the outflow of urban Beijing.

498 Since the NO<sub>3</sub>-N<sub>2</sub>O<sub>5</sub> chemical equilibrium favors NO<sub>3</sub> in summer with high temperature, the  
499 elevated NO<sub>3</sub> dominated the nocturnal degradation of BVOCs and could lead to efficient ON formation.  
500 Because the air masses in Beijing featured high NO<sub>x</sub>/BVOCs ratios (>10), our results suggest that the  
501 nocturnal NO<sub>3</sub> oxidation of BVOCs was NO<sub>x</sub>-dominated. Because of the extremely high NO<sub>x</sub>  
502 emissions, the formation of ON may not be sensitive to the reduction of NO<sub>x</sub> but rather to the change  
503 of unsaturated VOCs (e.g., BVOCs), which is similar to the daytime photochemical O<sub>3</sub> pollution (e.g.,  
504 Lu et al., 2010) diagnosed for this area. This suggests that the control of the unsaturated VOCs would  
505 moderate the O<sub>3</sub> pollution and ON particulate matter in parallel. Moreover, the reduction of NO<sub>x</sub> would

506 also be helpful to reduce the  $\text{pNO}_3^-$  formation via  $\text{N}_2\text{O}_5$  heterogeneous hydrolysis under such high  
507  $\text{NO}_x/\text{BVOCs}$  ratios (Edwards et al., 2017).

508

509 **Acknowledgements.** This work was supported by the National Natural Science Foundation of China  
510 (Grants No. 91544225, 41375124, 21522701, 41421064, 91744204), the National Science and  
511 Technology Support Program of China (No. 2014BAC21B01), the Strategic Priority Research  
512 Program of the Chinese Academy of Sciences (Grants No. XDB05010500), and the program on  
513 “Photochemical smog in China” financed by the Swedish Research Council (639-2013-6917). The  
514 authors gratefully acknowledge the Peking University and Gethenburg University science team for  
515 their technical support and discussions during the Changping campaign.

516

## 517 **Reference**

518

519 Allan, B. J., Carslaw, N., Coe, H., Burgess, R. A., and Plane, J. M. C.: Observations of the nitrate radical in the marine  
520 boundary layer, *J Atmos Chem*, 33, 129-154, Doi10.1023/A:1005917203307, 1999.

521 Bannan, T. J., Booth, A. M., Bacak, A., Muller, J. B. A., Leather, K. E., Le Breton, M., Jones, B., Young, D., Coe, H.,  
522 Allan, J., Visser, S., Slowik, J. G., Furger, M., Prevot, A. S. H., Lee, J., Dunmore, R. E., Hopkins, J. R., Hamilton,  
523 J. F., Lewis, A. C., Whalley, L. K., Sharp, T., Stone, D., Heard, D. E., Fleming, Z. L., Leigh, R., Shallcross, D.  
524 E., and Percival, C. J.: The first UK measurements of nitryl chloride using a chemical ionization mass  
525 spectrometer in central London in the summer of 2012, and an investigation of the role of Cl atom oxidation, *J*  
526 *Geophys Res-Atmos*, 120, 5638-5657, 10.1002/2014jd022629, 2015.

527 Benton, A. K., Langridge, J. M., Ball, S. M., Bloss, W. J., Dall'Osto, M., Nemitz, E., Harrison, R. M., and Jones, R.  
528 L.: Night-time chemistry above London: measurements of  $\text{NO}_3$  and  $\text{N}_2\text{O}_5$  from the BT Tower, *Atmos Chem*  
529 *Phys*, 10, 9781-9795, 10.5194/acp-10-9781-2010, 2010.

530 Bertram, T. H., and Thornton, J. A.: Toward a general parameterization of  $\text{N}_2\text{O}_5$  reactivity on aqueous particles: the  
531 competing effects of particle liquid water, nitrate and chloride, *Atmos Chem Phys*, 9, 8351-8363, 2009.

532 Bertram, T. H., Thornton, J. A., Riedel, T. P., Middlebrook, A. M., Bahreini, R., Bates, T. S., Quinn, P. K., and  
533 Coffman, D. J.: Direct observations of  $\text{N}_2\text{O}_5$  reactivity on ambient aerosol particles, *Geophys Res Lett*, 36, Art  
534 L19803.10.1029/2009gl040248, 2009.

535 Bohn, B., Corlett, G. K., Gillmann, M., Sanghavi, S., Stange, G., Tensing, E., Vrekoussis, M., Bloss, W. J., Clapp, L.  
536 J., Kortner, M., Dorn, H.-P., Monks, P. S., Platt, U., Plass-Dülmer, C., Mihalopoulos, N., Heard, D. E.,  
537 Clemmitshaw, K. C., Meixner, F. X., Prevot, A. S. H., and Schmitt, R.: Photolysis frequency measurement  
538 techniques: results of a comparison within the ACCENT project, *Atmos. Chem. Phys.*, 8, 5373–5391,  
539 doi:10.5194/acp-8-5373-2008, 2008.

540 Behnke, W., George, C., Scheer, V., and Zetzsch, C.: Production and decay of  $\text{ClNO}_2$ , from the reaction of gaseous  
541  $\text{N}_2\text{O}_5$  with NaCl solution: Bulk and aerosol experiments, *J Geophys Res-Atmos*, 102, 3795-3804, Doi  
542 10.1029/96jd03057, 1997.

543 Boyd, C. M., Nah, T., Xu, L., Berkemeier, T., and Ng, N. L.: Secondary Organic Aerosol (SOA) from Nitrate Radical  
544 Oxidation of Monoterpenes: Effects of Temperature, Dilution, and Humidity on Aerosol Formation, Mixing,  
545 and Evaporation, *Environ Sci Technol*, 51, 7831-7841, 2017.

546 Brown, S. S., Stark, H., and Ravishankara, A. R.: Applicability of the steady state approximation to the interpretation  
547 of atmospheric observations of  $\text{NO}_3$  and  $\text{N}_2\text{O}_5$ , *J Geophys Res-Atmos*, 108, Artn 4539. Doi  
548 10.1029/2003jd003407, 2003.

549 Brown, S. S., Ryerson, T. B., Wollny, A. G., Brock, C. A., Peltier, R., Sullivan, A. P., Weber, R. J., Dube, W. P.,  
550 Trainer, M., Meagher, J. F., Fehsenfeld, F. C., and Ravishankara, A. R.: Variability in nocturnal nitrogen oxide  
551 processing and its role in regional air quality, *Science*, 311, 67-70, DOI 10.1126/science.1120120, 2006.

552 Brown, S. S., Dube, W. P., Fuchs, H., Ryerson, T. B., Wollny, A. G., Brock, C. A., Bahreini, R., Middlebrook, A. M.,  
553 Neuman, J. A., Atlas, E., Roberts, J. M., Osthoff, H. D., Trainer, M., Fehsenfeld, F. C., and Ravishankara, A. R.:  
554 Reactive uptake coefficients for  $\text{N}_2\text{O}_5$  determined from aircraft measurements during the Second Texas Air  
555 Quality Study: Comparison to current model parameterizations, *J Geophys Res-Atmos*, 114, Artn D00f10. Doi  
556 10.1029/2008jd011679, 2009.

557 Brown, S. S., and Stutz, J.: Nighttime radical observations and chemistry, *Chem Soc Rev*, 41, 6405-6447, Doi  
558 10.1039/C2cs35181a, 2012.

559 Brown, S. S., Dube, W. P., Tham, Y. J., Zha, Q. Z., Xue, L. K., Poon, S., Wang, Z., Blake, D. R., Tsui, W., Parrish, D.  
560 D., and Wang, T.: Nighttime chemistry at a high altitude site above Hong Kong, *J Geophys Res-Atmos*, 121,  
561 2457-2475, 10.1002/2015jd024566, 2016.

562 Chang, W. L., Bhave, P. V., Brown, S. S., Riemer, N., Stutz, J., and Dabdub, D.: Heterogeneous Atmospheric  
563 Chemistry, Ambient Measurements, and Model Calculations of  $\text{N}_2\text{O}_5$ : A Review, *Aerosol Sci Tech*, 45, 665-695,  
564 2011.

565 DeCarlo, P. F., Kimmel, J., Trimborn, A., Northway, M., Jayne, J. T., Aiken, A., Gonin, M., Fuhrer, K., Horvath, T.,  
566 Docherty, K., Worsnop, D. R., and Jimenez, J. L.: Field-deployable, high-resolution, time-of-flight Aerosol Mass  
567 Spectrometer, *Anal. Chem.*, 78, 8281-8289, 2006.

568 de Gouw, J. and Warneke, C.: Measurements of volatile organic compounds in the earth's atmosphere using proton-  
569 transferreaction mass spectrometry, *Mass Spectrom. Rev.*, 26, 223-257, 2007.

570 Draxler, R. R., and G. D. Rolph: HYSPLIT (HYbrid Single-Particle Lagrangian Integrated Tracker) Model access  
571 via NOAA ARL Ready Website [Available at <http://www.arl.noaa.gov/ready/hysplit4.html>, NOAA Air  
572 Resources Laboratory, Silver Spring, MD]. 2003.

573 Edwards, P. M., Aikin, K. C., Dube, W. P., Fry, J. L., Gilman, J. B., de Gouw, J. A., Graus, M. G., Hanisco, T. F.,  
574 Holloway, J., Huber, G., Kaiser, J., Keutsch, F. N., Lerner, B. M., Neuman, J. A., Parrish, D. D., Peischl, J.,  
575 Pollack, I. B., Ravishankara, A. R., Roberts, J. M., Ryerson, T. B., Trainer, M., Veres, P. R., Wolfe, G. M.,  
576 Warneke, C., and Brown, S. S.: Transition from high- to low- $\text{NO}_x$  control of night-time oxidation in the  
577 southeastern US, *Nat Geosci*, 10, 490+, 10.1038/Ngeo2976, 2017.

578 Faxon, C. B., Bean, J. K., and Ruiz, L. H.: Inland Concentrations of  $\text{Cl}_2$  and  $\text{ClNO}_2$  in Southeast Texas suggest  
579 chlorine chemistry significantly contributes to atmospheric reactivity, *Atmosphere*, 6, 1487-1506, 2015.

580 Finlayson-Pitts, B. J., Ezell, M. J., and Pitts, J. N.: Formation of Chemically Active Chlorine Compounds by  
581 Reactions of Atmospheric NaCl Particles with Gaseous  $N_2O_5$  and  $ClONO_2$ , *Nature*, 337, 241-244, DOI  
582 10.1038/337241a0, 1989.

583 Fry, J. L., Kiendler-Scharr, A., Rollins, A. W., Wooldridge, P. J., Brown, S. S., Fuchs, H., Dube, W., Mensah, A., dal  
584 Maso, M., Tillmann, R., Dorn, H. P., Brauers, T., and Cohen, R. C.: Organic nitrate and secondary organic  
585 aerosol yield from  $NO_3$  oxidation of beta-pinene evaluated using a gas-phase kinetics/aerosol partitioning model,  
586 *Atmos Chem Phys*, 9, 1431-1449, 2009.

587 Gaston, C. J., Thornton, J. A., and Ng, N. L.: Reactive uptake of  $N_2O_5$  to internally mixed inorganic and organic  
588 particles: the role of organic carbon oxidation state and inferred organic phase separations, *Atmos Chem Phys*,  
589 14, 5693-5707, 10.5194/acp-14-5693-2014, 2014.

590 Geyer, A., Aliche, B., Konrad, S., Schmitz, T., Stutz, J., and Platt, U.: Chemistry and oxidation capacity of the nitrate  
591 radical in the continental boundary layer near Berlin, *J Geophys Res-Atmos*, 106, 8013-8025, Doi  
592 10.1029/2000jd900681, 2001.

593 Goliff, W. S., Stockwell, W. R., and Lawson, C. V.: The regional atmospheric chemistry mechanism, version 2, *Atmos*  
594 *Environ*, 68, 174-185, 2013.

595 Grzinic, G., Bartels-Rausch, T., Berkemeier, T., Turler, A., and Ammann, M.: Viscosity controls humidity dependence  
596 of  $N_2O_5$  uptake to citric acid aerosol, *Atmos Chem Phys*, 15, 13615-13625, 2015.

597 Hallquist, M., Stewart, D. J., Stephenson, S. K., and Cox, R. A.: Hydrolysis of  $N_2O_5$  on sub-micron sulfate aerosols,  
598 *Phys Chem Chem Phys*, 5, 3453-3463, Doi 10.1039/B301827j, 2003.

599 Hallquist, M., Munthe, J., Hu, M., Wang, T., Chan, C. K., Gao, J., Boman, J., Guo, S., Hallquist, A. M., Mellqvist, J.,  
600 Moldanova, J., Pathak, R. K., Pettersson, J. B. C., Pleijel, H., Simpson, D., and Thynell, M.: Photochemical  
601 smog in China: scientific challenges and implications for air-quality policies, *Natl Sci Rev*, 3, 401-403,  
602 10.1093/nsr/nww080, 2016.

603 Kiendler-Scharr, A., Mensah, A. A., Friese, E., Topping, D., Nemitz, E., Prevot, A. S. H., Aijala, M., Allan, J.,  
604 Canonaco, F., Canagaratna, M., Carbone, S., Crippa, M., Dall'Osto, M., Day, D. A., De Carlo, P., Di Marco, C.  
605 F., Elbern, H., Eriksson, A., Freney, E., Hao, L., Herrmann, H., Hildebrandt, L., Hillamo, R., Jimenez, J. L.,  
606 Laaksonen, A., McFiggans, G., Mohr, C., O'Dowd, C., Otjes, R., Ovadnevaite, J., Pandis, S. N., Poulain, L.,  
607 Schlag, P., Sellegri, K., Swietlicki, E., Tiitta, P., Vermeulen, A., Wahner, A., Worsnop, D., and Wu, H. C.:  
608 Ubiquity of organic nitrates from nighttime chemistry in the European submicron aerosol, *Geophys Res Lett*,  
609 43, 7735-7744, 2016.

610 Le Breton, M., Bacak, A., Muller, J. B. A., Bannan, T. J., Kennedy, O., Ouyang, B., Xiao, P., Bauguitte, S. J. B.,  
611 Shallcross, D. E., Jones, R. L., Daniels, M. J. S., Ball, S. M., and Percival, C. J.: The first airborne comparison  
612 of  $N_2O_5$  measurements over the UK using a CIMS and BBCEAS during the RONOCO campaign, *Anal*  
613 *Methods-Uk*, 6, 9731-9743, 10.1039/c4ay02273d, 2014.

614 Le Breton, M., Hallquist, Å. M., Pathak, R. K., Simpson, D., Wang, Y., Johansson, J., Zheng, J., Yang, Y., Shang, D.,  
615 Wang, H., Liu, Q., Chan, C., Wang, T., Bannan, T. J., Priestley, M., Percival, C. J., Shallcross, D. E., Lu, K.,  
616 Guo, S., Hu, M., and Hallquist, M.: Chlorine oxidation of VOCs at a semi-rural site in Beijing: Significant



617 chlorine liberation from ClNO<sub>2</sub> and subsequent gas and particle phase Cl-VOC production, *Atmos. Chem. Phys.*  
618 *Discuss.*, 2018, 1-25, 2018.

619 Li, S. W., Liu, W. Q., Xie, P. H., Qin, M., and Yang, Y. J.: Observation of Nitrate Radical in the Nocturnal Boundary  
620 Layer During a Summer Field Campaign in Pearl River Delta, China, *Terr Atmos Ocean Sci*, 23, 39-48, Doi  
621 10.3319/Tao.2011.07.26.01(a), 2012.

622 Li, Q. Y., Zhang, L., Wang, T., Tham, Y. J., Ahmadov, R., Xue, L. K., Zhang, Q., and Zheng, J. Y.: Impacts of  
623 heterogeneous uptake of dinitrogen pentoxide and chlorine activation on ozone and reactive nitrogen  
624 partitioning: improvement and application of the WRF-Chem model in southern China, *Atmos Chem Phys*, 16,  
625 14875-14890, 10.5194/acp-16-14875-2016, 2016.

626 Liu, X. G., Gu, J. W., Li, Y. P., Cheng, Y. F., Qu, Y., Han, T. T., Wang, J. L., Tian, H. Z., Chen, J., and Zhang, Y. H.:  
627 Increase of aerosol scattering by hygroscopic growth: Observation, modeling, and implications on visibility,  
628 *Atmos Res*, 132, 91-101, 10.1016/j.atmosres.2013.04.007, 2013.

629 Liu, M. X., Song, Y., Zhou, T., Xu, Z. Y., Yan, C. Q., Zheng, M., Wu, Z. J., Hu, M., Wu, Y. S., and Zhu, T.: Fine  
630 particle pH during severe haze episodes in northern China, *Geophys Res Lett*, 44, 5213-5221,  
631 10.1002/2017gl073210, 2017.

632 Lopez-Hilfiker, F. D., Mohr, C., Ehn, M., Rubach, F., Kleist, E., Wildt, J., Mentel, T. F., Lutz, A., Hallquist, M.,  
633 Worsnop, D., and Thornton, J. A.: A novel method for online analysis of gas and particle composition:  
634 description and evaluation of a Filter Inlet for Gases and AEROSols (FIGAERO), *Atmos Meas Tech*, 7, 983-  
635 1001, 10.5194/amt-7-983-2014, 2014.

636 Lu, K. D., Zhang, Y. H., Su, H., Brauers, T., Chou, C. C., Hofzumahaus, A., Liu, S. C., Kita, K., Kondo, Y., Shao,  
637 M., Wahner, A., Wang, J. L., Wang, X. S., and Zhu, T.: Oxidant (O<sub>3</sub> + NO<sub>2</sub>) production processes and formation  
638 regimes in Beijing, *J Geophys Res-Atmos*, 115, 2010.

639 McLaren, R., Wojtal, P., Majonis, D., McCourt, J., Halla, J. D., and Brook, J.: NO<sub>3</sub> radical measurements in a polluted  
640 marine environment: links to ozone formation, *Atmos Chem Phys*, 10, 4187-4206, 10.5194/acp-10-4187-2010,  
641 2010.

642 Mentel, T. F., Sohn, M., and Wahner, A.: Nitrate effect in the heterogeneous hydrolysis of dinitrogen pentoxide on  
643 aqueous aerosols, *Phys Chem Chem Phys*, 1, 5451-5457, Doi 10.1039/A905338g, 1999.

644 Mielke, L. H., Furgeson, A., and Osthoff, H. D.: Observation of ClNO<sub>2</sub> in a Mid-Continental Urban Environment,  
645 *Environ Sci Technol*, 45, 8889-8896, 10.1021/es201955u, 2011.

646 Mielke, L. H., Stutz, J., Tsai, C., Hurlock, S. C., Roberts, J. M., Veres, P. R., Froyd, K. D., Hayes, P. L., Cubison, M.  
647 J., Jimenez, J. L., Washenfelder, R. A., Young, C. J., Gilman, J. B., de Gouw, J. A., Flynn, J. H., Grossberg, N.,  
648 Lefer, B. L., Liu, J., Weber, R. J., and Osthoff, H. D.: Heterogeneous formation of nitryl chloride and its role as  
649 a nocturnal NO<sub>x</sub> reservoir species during CalNex-LA 2010, *J Geophys Res-Atmos*, 118, 10638-10652, Doi  
650 10.1002/Jgrd.50783, 2013.

651 Morgan, W. T., Ouyang, B., Allan, J. D., Aruffo, E., Di Carlo, P., Kennedy, O. J., Lowe, D., Flynn, M. J., Rosenberg,  
652 P. D., Williams, P. I., Jones, R., McFiggans, G. B., and Coe, H.: Influence of aerosol chemical composition on

653 N<sub>2</sub>O<sub>5</sub> uptake: airborne regional measurements in northwestern Europe, *Atmos Chem Phys*, 15, 973-990, DOI  
654 10.5194/acp-15-973-2015, 2015.

655 Ng, N. L., Kwan, A. J., Surratt, J. D., Chan, A. W. H., Chhabra, P. S., Sorooshian, A., Pye, H. O. T., Crounse, J. D.,  
656 Wennberg, P. O., Flagan, R. C., and Seinfeld, J. H.: Secondary organic aerosol (SOA) formation from reaction  
657 of isoprene with nitrate radicals (NO<sub>3</sub>), *Atmos Chem Phys*, 8, 4117-4140, 2008.

658 Ng, N. L., Brown, S. S., Archibald, A. T., Atlas, E., Cohen, R. C., Crowley, J. N., Day, D. A., Donahue, N. M., Fry,  
659 J. L., Fuchs, H., Griffin, R. J., Guzman, M. I., Herrmann, H., Hodzic, A., Iinuma, Y., Jimenez, J. L., Kiendler-  
660 Scharr, A., Lee, B. H., Luecken, D. J., Mao, J. Q., McLaren, R., Mutzel, A., Osthoff, H. D., Ouyang, B., Picquet-  
661 Varrault, B., Platt, U., Pye, H. O. T., Rudich, Y., Schwantes, R. H., Shiraiwa, M., Stutz, J., Thornton, J. A.,  
662 Tilgner, A., Williams, B. J., and Zaveri, R. A.: Nitrate radicals and biogenic volatile organic compounds:  
663 oxidation, mechanisms, and organic aerosol, *Atmos Chem Phys*, 17, 2103-2162, 10.5194/acp-17-2103-2017,  
664 2017.

665 Osthoff, H. D., Roberts, J. M., Ravishankara, A. R., Williams, E. J., Lerner, B. M., Sommariva, R., Bates, T. S.,  
666 Coffman, D., Quinn, P. K., Dibb, J. E., Stark, H., Burkholder, J. B., Talukdar, R. K., Meagher, J., Fehsenfeld, F.  
667 C., and Brown, S. S.: High levels of nitryl chloride in the polluted subtropical marine boundary layer, *Nat Geosci*,  
668 1, 324-328, Doi 10.1038/Ngeo177, 2008.

669 Phillips, G. J., Thieser, J., Tang, M. J., Sobanski, N., Schuster, G., Fachinger, J., Drewnick, F., Borrmann, S.,  
670 Bingemer, H., Lelieveld, J., and Crowley, J. N.: Estimating N<sub>2</sub>O<sub>5</sub> uptake coefficients using ambient  
671 measurements of NO<sub>3</sub>, N<sub>2</sub>O<sub>5</sub>, ClNO<sub>2</sub> and particle-phase nitrate, *Atmos Chem Phys*, 16, 13231-13249,  
672 10.5194/acp-16-13231-2016, 2016.

673 Platt, U., Perner, D., Winer, A. M., Harris, G. W., and Pitts, J. N.: Detection of NO<sub>3</sub> in the Polluted Troposphere by  
674 Differential Optical-Absorption, *Geophys Res Lett*, 7, 89-92, Doi 10.1029/G1007i001p00089, 1980.

675 Pye, H. O. T., Chan, A. W. H., Barkley, M. P., and Seinfeld, J. H.: Global modeling of organic aerosol: the importance  
676 of reactive nitrogen (NO<sub>x</sub> and NO<sub>3</sub>), *Atmos Chem Phys*, 10, 11261-11276, 2010.

677 Riedel, T. P., Bertram, T. H., Ryder, O. S., Liu, S., Day, D. A., Russell, L. M., Gaston, C. J., Prather, K. A., and  
678 Thornton, J. A.: Direct N<sub>2</sub>O<sub>5</sub> reactivity measurements at a polluted coastal site, *Atmos Chem Phys*, 12, 2959-  
679 2968, DOI 10.5194/acp-12-2959-2012, 2012.

680 Riedel, T. P., Wolfe, G. M., Danas, K. T., Gilman, J. B., Kuster, W. C., Bon, D. M., Vlasenko, A., Li, S. M., Williams,  
681 E. J., Lerner, B. M., Veres, P. R., Roberts, J. M., Holloway, J. S., Lefer, B., Brown, S. S., and Thornton, J. A.:  
682 An MCM modeling study of nitryl chloride (ClNO<sub>2</sub>) impacts on oxidation, ozone production and nitrogen oxide  
683 partitioning in polluted continental outflow, *Atmos Chem Phys*, 14, 3789-3800, 10.5194/acp-14-3789-2014,  
684 2014.

685 Riemer, N., Vogel, H., Vogel, B., Anttila, T., Kiendler-Scharr, A., and Mentel, T. F.: Relative importance of organic  
686 coatings for the heterogeneous hydrolysis of N<sub>2</sub>O<sub>5</sub> during summer in Europe, *J Geophys Res-Atmos*, 114, 2009.

687 Roberts, J. M., Osthoff, H. D., Brown, S. S., Ravishankara, A. R., Coffman, D., Quinn, P., and Bates, T.: Laboratory  
688 studies of products of N<sub>2</sub>O<sub>5</sub> uptake on Cl<sup>-</sup> containing substrates, *Geophys Res Lett*, 36, Artn L20808.  
689 10.1029/2009gl040448, 2009.

690 Rollins, A. W., Kiendler-Scharr, A., Fry, J. L., Brauers, T., Brown, S. S., Dorn, H. P., Dube, W. P., Fuchs, H., Mensah,  
691 A., Mentel, T. F., Rohrer, F., Tillmann, R., Wegener, R., Wooldridge, P. J., and Cohen, R. C.: Isoprene oxidation  
692 by nitrate radical: alkyl nitrate and secondary organic aerosol yields, *Atmos Chem Phys*, 9, 6685-6703, 2009.

693 Sarwar, G., Simon, H., Xing, J., and Mathur, R.: Importance of tropospheric ClNO<sub>2</sub> chemistry across the Northern  
694 Hemisphere, *Geophys Res Lett*, 41, 4050-4058, 10.1002/2014gl059962, 2014.

695 Spittler, M., Barnes, I., Bejan, I., Brockmann, K. J., Benter, T., and Wirtz, K.: Reactions of NO<sub>3</sub> radicals with  
696 limonene and alpha-pinene: Product and SOA formation, *Atmos Environ*, 40, S116-S127,  
697 10.1016/j.atmosenv.2005.09.093, 2006.

698 Stutz, J., Wong, K. W., Lawrence, L., Ziemba, L., Flynn, J. H., Rappengluck, B., and Lefer, B.: Nocturnal NO<sub>3</sub> radical  
699 chemistry in Houston, TX, *Atmos Environ*, 44, 4099-4106, 10.1016/j.atmosenv.2009.03.004, 2010.

700 Su, X., Tie, X. X., Li, G. H., Cao, J. J., Huang, R. J., Feng, T., Long, X., and Xu, R. G.: Effect of hydrolysis of N<sub>2</sub>O<sub>5</sub>  
701 on nitrate and ammonium formation in Beijing China: WRF-Chem model simulation, *Sci Total Environ*, 579,  
702 221-229, 10.1016/j.scitotenv.2016.11.125, 2017.

703 Tan, Z., Fuchs, H., Lu, K., Hofzumahaus, A., Bohn, B., Broch, S., Dong, H., Gomm, S., Häsel, R., He, L., Holland,  
704 F., Li, X., Liu, Y., Lu, S., Rohrer, F., Shao, M., Wang, B., Wang, M., Wu, Y., Zeng, L., Zhang, Y., Wahner, A.,  
705 and Zhang, Y.: Radical chemistry at a rural site (Wangdu) in the North China Plain: observation and model  
706 calculations of OH, HO<sub>2</sub> and RO<sub>2</sub> radicals, *Atmos. Chem. Phys.*, 17, 663-690, 10.5194/acp-17-663-2017, 2017.

707 Tang, M. J., Schuster, G., and Crowley, J. N.: Heterogeneous reaction of N<sub>2</sub>O<sub>5</sub> with illite and Arizona test dust  
708 particles, *Atmos Chem Phys*, 14, 245-254, 2014.

709 Tang, M. J., Thieser, J., Schuster, G., and Crowley, J. N.: Kinetics and mechanism of the heterogeneous reaction of  
710 N<sub>2</sub>O<sub>5</sub> with mineral dust particles, *Phys Chem Chem Phys*, 14, 8551-8561, 2012.

711 Tang, M. J., Huang, X., Lu, K. D., Ge, M. F., Li, Y. J., Cheng, P., Zhu, T., Ding, A. J., Zhang, Y. H., Gligorovski, S.,  
712 Song, W., Ding, X., Bi, X. H., and Wang, X. M.: Heterogeneous reactions of mineral dust aerosol: implications  
713 for tropospheric oxidation capacity, *Atmos Chem Phys*, 17, 11727-11777, 10.5194/acp-17-11727-2017, 2017.

714 Tham, Y. J., Wang, Z., Li, Q. Y., Yun, H., Wang, W. H., Wang, X. F., Xue, L. K., Lu, K. D., Ma, N., Bohn, B., Li, X.,  
715 Kecorius, S., Gross, J., Shao, M., Wiedensohler, A., Zhang, Y. H., and Wang, T.: Significant concentrations of  
716 nitryl chloride sustained in the morning: investigations of the causes and impacts on ozone production in a  
717 polluted region of northern China, *Atmos Chem Phys*, 16, 14959-14977, 10.5194/acp-16-14959-2016, 2016.

718 Thornton, J. A., Braban, C. F., and Abbatt, J. P. D.: N<sub>2</sub>O<sub>5</sub> hydrolysis on sub-micron organic aerosols: the effect of  
719 relative humidity, particle phase, and particle size, *Phys Chem Chem Phys*, 5, 4593-4603, Doi  
720 10.1039/B307498f, 2003.

721 Thornton, J. A., and Abbatt, J. P. D.: N<sub>2</sub>O<sub>5</sub> reaction on submicron sea salt aerosol: Kinetics, products, and the effect  
722 of surface active organics, *J Phys Chem A*, 109, 10004-10012, Doi 10.1021/Jp054183t, 2005.

723 Thornton, J. A., Kercher, J. P., Riedel, T. P., Wagner, N. L., Cozic, J., Holloway, J. S., Dube, W. P., Wolfe, G. M.,  
724 Quinn, P. K., Middlebrook, A. M., Alexander, B., and Brown, S. S.: A large atomic chlorine source inferred from  
725 mid-continental reactive nitrogen chemistry, *Nature*, 464, 271-274, Doi 10.1038/Nature08905, 2010.

726 Wagner, N. L., Riedel, T. P., Young, C. J., Bahreini, R., Brock, C. A., Dube, W. P., Kim, S., Middlebrook, A. M.,  
727 Ozturk, F., Roberts, J. M., Russo, R., Sive, B., Swarthout, R., Thornton, J. A., VandenBoer, T. C., Zhou, Y., and  
728 Brown, S. S.: N<sub>2</sub>O<sub>5</sub> uptake coefficients and nocturnal NO<sub>2</sub> removal rates determined from ambient wintertime  
729 measurements, *J Geophys Res-Atmos*, 118, 9331-9350, Doi 10.1002/Jgrd.50653, 2013.

730 Wahner, A., Mentel, T. F., and Sohn, M.: Gas-phase reaction of N<sub>2</sub>O<sub>5</sub> with water vapor: Importance of heterogeneous  
731 hydrolysis of N<sub>2</sub>O<sub>5</sub> and surface desorption of HNO<sub>3</sub> in a large teflon chamber, *Geophys Res Lett*, 25, 2169-  
732 2172, Doi 10.1029/98gl51596, 1998.

733 Wang, S. S., Shi, C. Z., Zhou, B., Zhao, H., Wang, Z. R., Yang, S. N., and Chen, L. M.: Observation of NO<sub>3</sub> radicals  
734 over Shanghai, China, *Atmos Environ*, 70, 401-409, DOI 10.1016/j.atmosenv.2013.01.022, 2013.

735 Wang, M., Shao, M., Chen, W., Yuan, B., Lu, S., Zhang, Q., Zeng, L., and Wang, Q.: A temporally and spatially  
736 resolved validation of emission inventories by measurements of ambient volatile organic compounds in Beijing,  
737 China, *Atmos Chem Phys*, 14, 5871-5891, 10.5194/acp-14-5871-2014, 2014.

738 Wang, D., Hu, R. Z., Xie, P. H., Liu, J. G., Liu, W. Q., Qin, M., Ling, L. Y., Zeng, Y., Chen, H., Xing, X. B., Zhu, G.  
739 L., Wu, J., Duan, J., Lu, X., and Shen, L. L.: Diode laser cavity ring-down spectroscopy for in situ measurement  
740 of NO<sub>3</sub> radical in ambient air, *J Quant Spectrosc Ra*, 166, 23-29, 10.1016/j.jqsrt.2015.07.005, 2015.

741 Wang, H. C., and Lu, K. D.: Determination and Parameterization of the Heterogeneous Uptake Coefficient of  
742 Dinitrogen Pentoxide (N<sub>2</sub>O<sub>5</sub>), *Prog Chem*, 28, 917-933, 10.7536/Pc151225, 2016.

743 Wang, T., Tham, Y. J., Xue, L. K., Li, Q. Y., Zha, Q. Z., Wang, Z., Poon, S. C. N., Dube, W. P., Blake, D. R., Louie,  
744 P. K. K., Luk, C. W. Y., Tsui, W., and Brown, S. S.: Observations of nitryl chloride and modeling its source and  
745 effect on ozone in the planetary boundary layer of southern China, *J Geophys Res-Atmos*, 121, 2476-2489,  
746 10.1002/2015jd024556, 2016.

747 Wang, H. C., Chen, J., and Lu, K. D.: Development of a portable cavity-enhanced absorption spectrometer for the  
748 measurement of ambient NO<sub>3</sub> and N<sub>2</sub>O<sub>5</sub>: experimental setup, lab characterizations, and field applications in a  
749 polluted urban environment, *Atmos Meas Tech*, 10, 1465-1479, 10.5194/amt-10-1465-2017, 2017a.

750 Wang, H. C., Lu, K. D., Tan, Z. F., Sun, K., Li, X., Hu, M., Shao, M., Zeng, L. M., Zhu, T., and Zhang, Y. H.:  
751 Model simulation of NO<sub>3</sub>, N<sub>2</sub>O<sub>5</sub> and ClNO<sub>2</sub> at a rural site in Beijing during CAREBeijing-2006, *Atmos Res*,  
752 196, 97-107, 10.1016/j.atmosres.2017.06.013, 2017b.

753 Wang, H. C., Lu, K. D., Chen, X. R., Zhu, Q. D., Chen, Q., Guo, S., Jiang, M. Q., Li, X., Shang, D. J., Tan, Z. F.:  
754 High N<sub>2</sub>O<sub>5</sub> concentrations observed in urban Beijing: Implications of a large nitrate formation pathway.,  
755 *Environ. Sci. Technol. Lett.*, 10, doi: 10.1021/acs.estlett.7b00341, 2017c.

756 Wang, X. F., Wang, H., Xue, L. K., Wang, T., Wang, L. W., Gu, R. R., Wang, W. H., Tham, Y. J., Wang, Z., Yang, L.  
757 X., Chen, J. M., and Wang, W. X.: Observations of N<sub>2</sub>O<sub>5</sub> and ClNO<sub>2</sub> at a polluted urban surface site in North  
758 China: High N<sub>2</sub>O<sub>5</sub> uptake coefficients and low ClNO<sub>2</sub> product yields, *Atmos Environ*, 156, 125-134,  
759 10.1016/j.atmosenv.2017.02.035, 2017.

760 Wang, Z., Wang, W. H., Tham, Y. J., Li, Q. Y., Wang, H., Wen, L., Wang, X. F., and Wang, T.: Fast heterogeneous  
761 N<sub>2</sub>O<sub>5</sub> uptake and ClNO<sub>2</sub> production in power plant and industrial plumes observed in the nocturnal residual  
762 layer over the North China Plain, *Atmos Chem Phys*, 17, 12361-12378, 2017. 10.5194/acp-17-12361-2017

763 Wayne, R. P., Barnes, I., Biggs, P., Burrows, J. P., Canosamas, C. E., Hjorth, J., Lebras, G., Moortgat, G. K., Perner,  
764 D., Poulet, G., Restelli, G., and Sidebottom, H.: The Nitrate Radical - Physics, Chemistry, and the Atmosphere,  
765 Atmos Environ a-Gen, 25, 1-203, Doi 10.1016/0960-1686(91)90192-A, 1991.

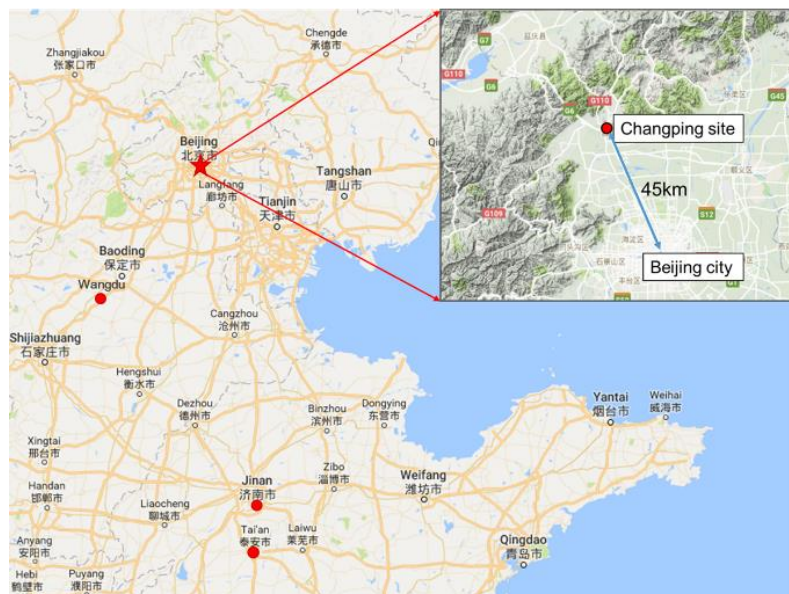
766 Xue, L. K., Saunders, S. M., Wang, T., Gao, R., Wang, X. F., Zhang, Q. Z., and Wang, W. X.: Development of a  
767 chlorine chemistry module for the Master Chemical Mechanism, Geosci Model Dev, 8, 3151-3162,  
768 10.5194/gmd-8-3151-2015, 2015.

769 Ye, N. N. L., K. D. Dong, H. B. Wu, Y. S. Zeng, L. M and Zhang, Y. H.: A study of the Water-Soluble Inorganic Salts  
770 and Their Gases Precursors at Wangdu Site in the Summer Time, Acta Scientiarum Naturalium Universitatis,  
771 52, p1109-1117, doi.org/10.13209/j.0479-8023.2016.116, 2016.

772 Yue, D. L., Hu, M., Wu, Z. J., Wang, Z. B., Guo, S., Wehner, B., Nowak, A., Achtert, P., Wiedensohler, A., Jung, J.,  
773 Kim, Y. J., and Liu, S.: Characteristics of aerosol size distributions and new particle formation in the summer in  
774 Beijing, J Geophys Res-Atmos, 114, Artn D00g1210.1029/2008jd010894, 2009.

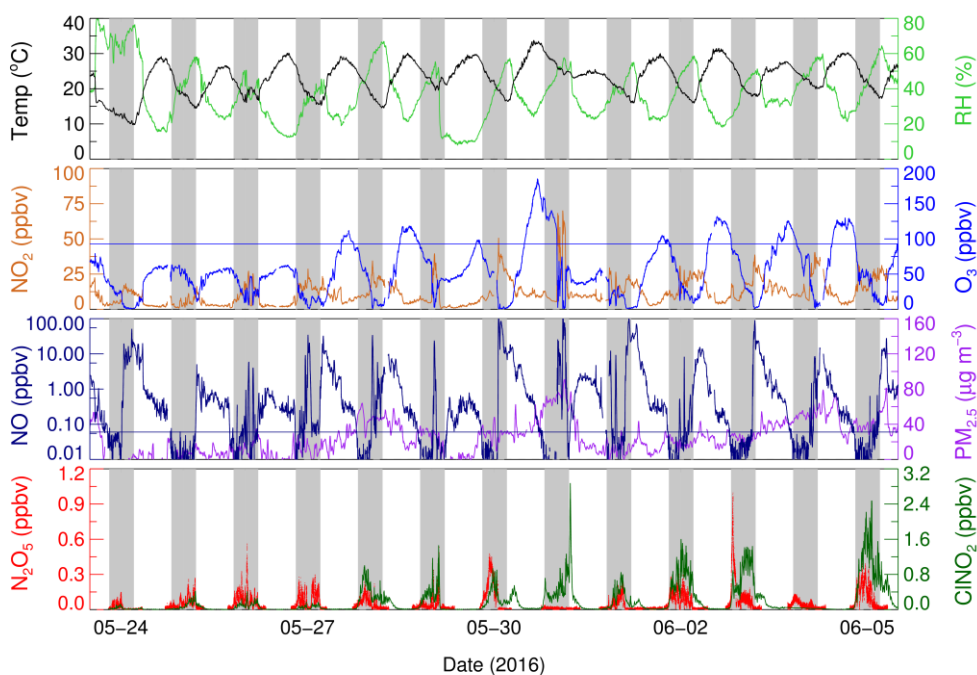
775 Zheng, J., Hu, M., Du, Z. F., Shang, D. J., Gong, Z. H., Qin, Y. H., Fang, J. Y., Gu, F. T., Li, M. R., Peng, J. F., Li, J.,  
776 Zhang, Y. Q., Huang, X. F., He, L. Y., Wu, Y. S., and Guo, S.: Influence of biomass burning from South Asia at  
777 a high-altitude mountain receptor site in China, Atmos Chem Phys, 17, 6853-6864, 10.5194/acp-17-6853-2017,  
778 2017.

779



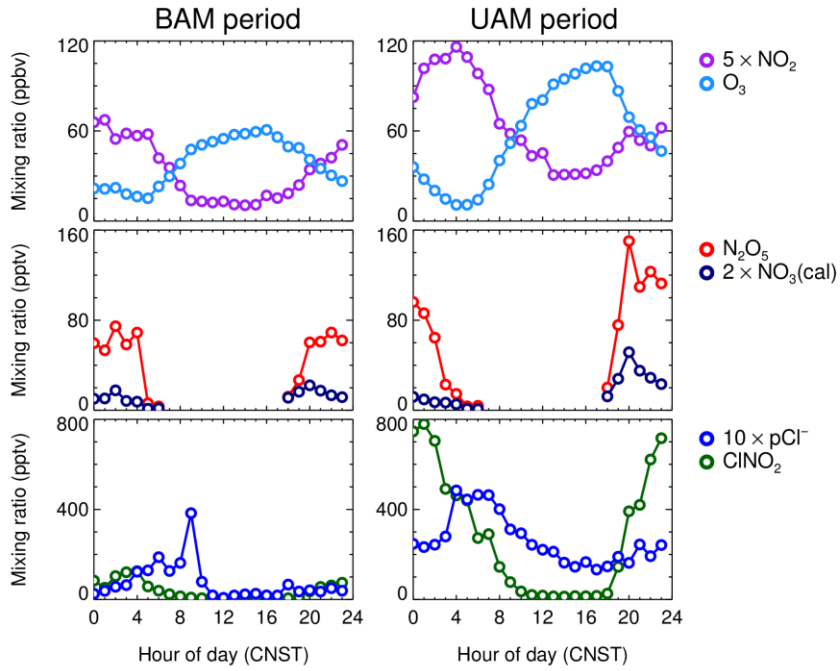
780

781 **Figure 1.** Map of Beijing and surrounding area. The red star shows the location of the Changping site,  
 782 and red dots show other sites where previous  $\text{N}_2\text{O}_5$  measurements were conducted in the North China  
 783 Plain (NCP), including Wangdu, Jinan and Mt. Tai (Tai' an).



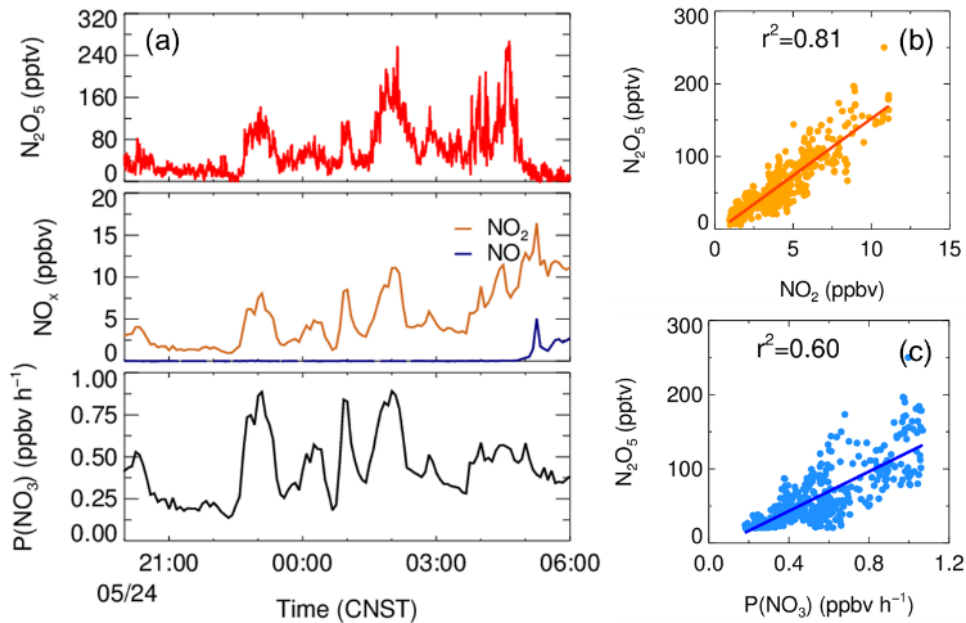
784

785 **Figure 2.** Time series of  $\text{N}_2\text{O}_5$ ,  $\text{ClNO}_2$  and other relevant parameters. The blue line in the  $\text{O}_3$  panel  
 786 denotes Chinese national air quality standard for  $\text{O}_3$  (ca. 93 ppbv for the surface conditions). The  
 787 black line in the  $\text{NO}$  panel denotes 0.06 ppbv.



788

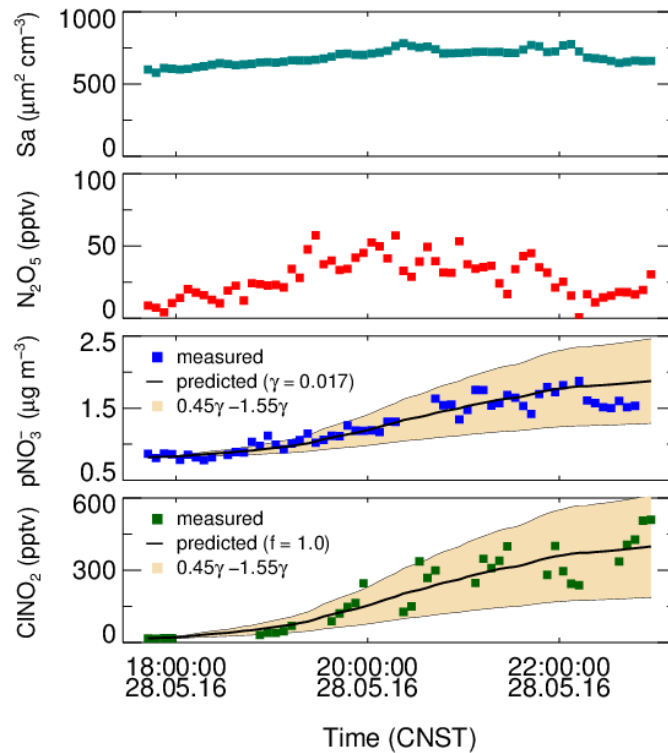
789 **Figure 3.** Mean diurnal profiles of  $5\times\text{NO}_2$ ,  $\text{O}_3$ ,  $\text{N}_2\text{O}_5$ ,  $2\times\text{NO}_3$  (calculated),  $\text{ClNO}_2$ , and  $10\times\text{pCl}^-$ . The  
 790 left three panels depict the background air mass (BAM) period and the right three panels depict the  
 791 urban air mass (UAM) period.



792

793 **Figure 4.** The correlation of the mixing ratio of  $\text{N}_2\text{O}_5$  and  $\text{NO}_2$  and the production rate of  $\text{NO}_3$  on the  
 794 night of May 24.

795

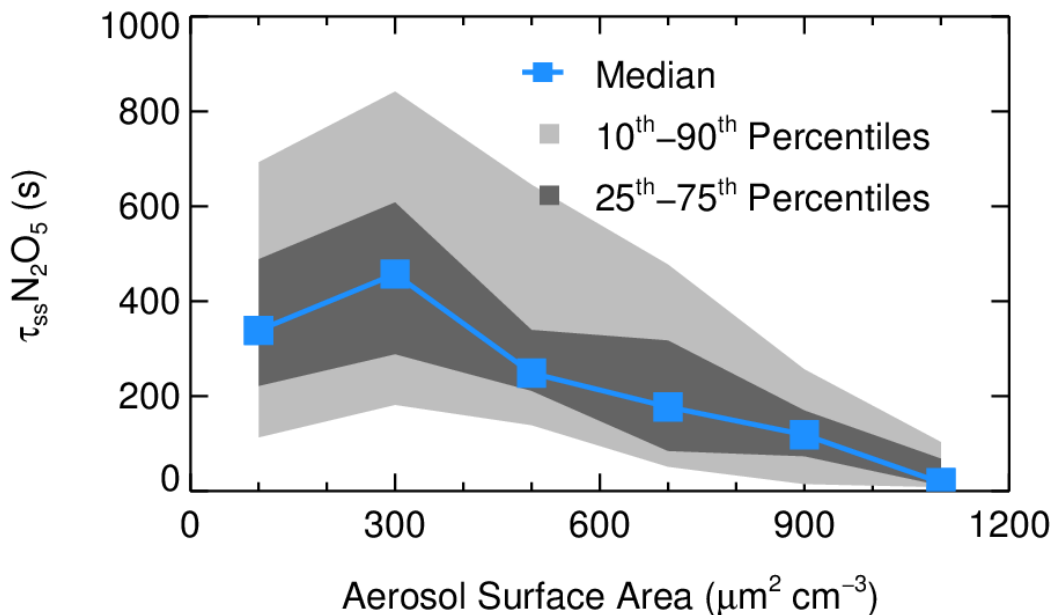


796

797 **Figure 5.** The best fit of  $\gamma$  and  $f$  to reproduce the observed  $\text{ClNO}_2$  and  $\text{pNO}_3^-$  with an offset on May 28.

798 The black lines are the predicted results of the integrated  $\text{NO}_3^-$  and  $\text{ClNO}_2$  by using the observed  $S_a$

799 and  $\text{N}_2\text{O}_5$ .



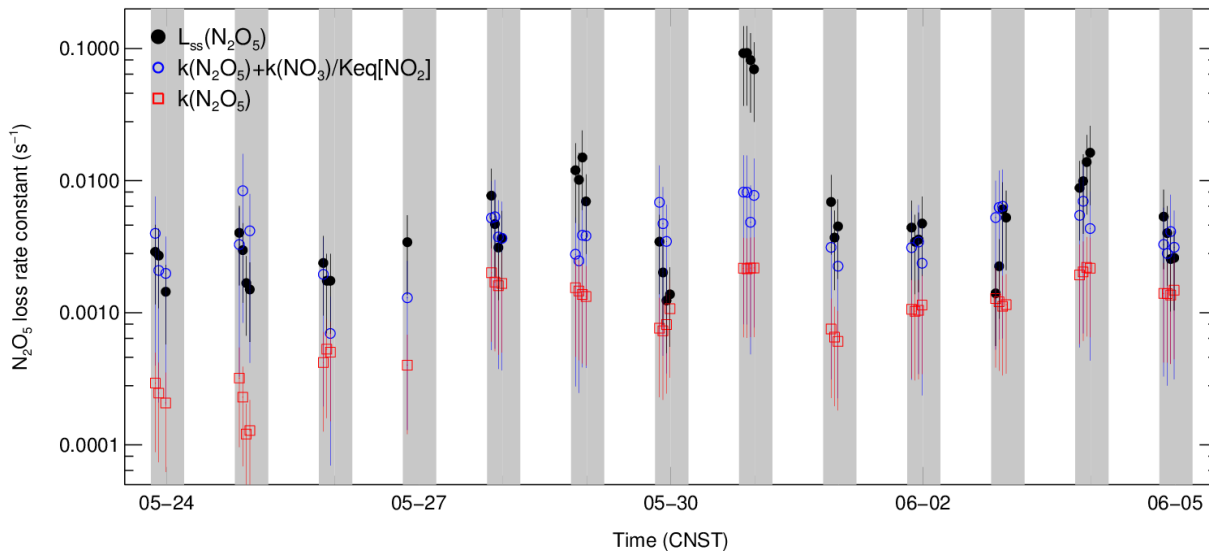
800

801 **Figure 6.** The dependence of  $\text{N}_2\text{O}_5$  lifetime on aerosol surface area. Data were selected from 20:00 to

802 04:00 and are shown as medians, 25 - 75<sup>th</sup> percentile ranges, and 10 - 90<sup>th</sup> percentile ranges, as shown

803 in the legend.

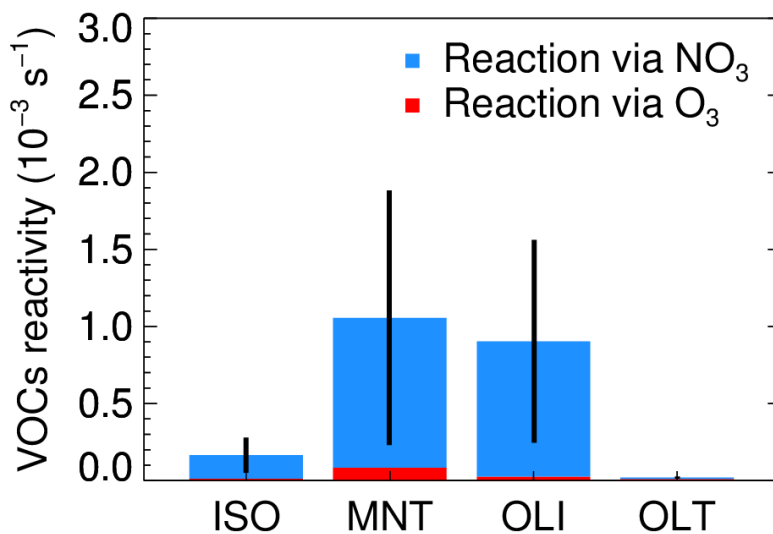




804

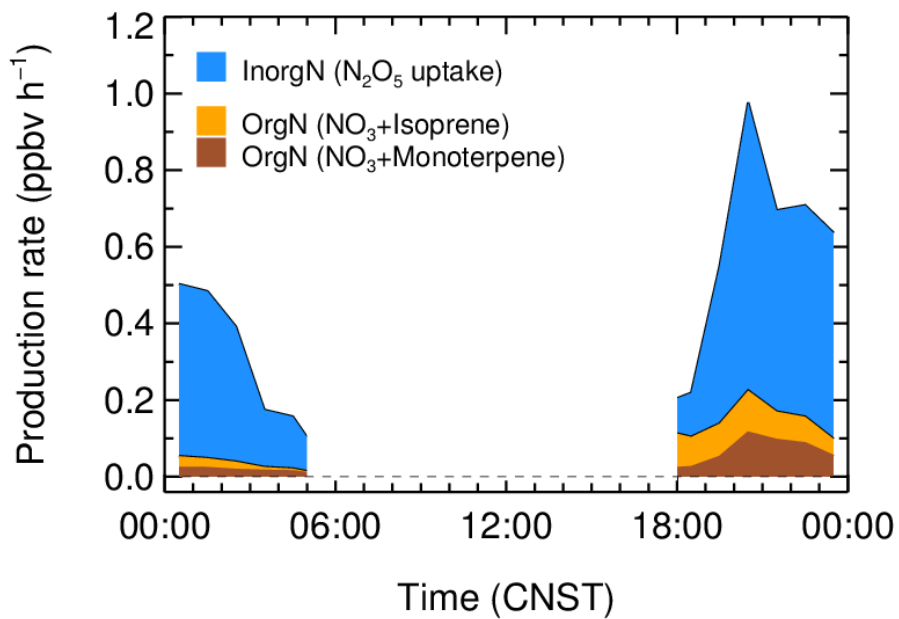
805 **Figure 7.** Time series of the individual  $N_2O_5$  loss terms and the loss rate constant of  $N_2O_5$  in steady  
 806 state ( $L_{ss}(N_2O_5)$ ).

807



808

809 **Figure 8.** The nighttime VOCs reactivity of  $NO_3$  and  $O_3$  (defined as the first order loss rate of VOCs  
 810 initialized by oxidants, include  $NO_3$  and  $O_3$ ); the VOCs are classified as isoprene (ISO), monoterpene  
 811 (MNT), the terminal alkenes (OLT) and the internal alkenes (OLI). The data were selected from 20:00  
 812 to the next day 04:00.



813

814 **Figure 9.** The nighttime production rate of organic and inorganic nitrates; the inorganic nitrates were  
 815 calculated from the N<sub>2</sub>O<sub>5</sub> heterogeneous hydrolysis, and the ON were calculated by the NO<sub>3</sub> reacted  
 816 with isoprene and monoterpene.

817

818

819 **Table 1.** The observed gas and particle parameters used in this analysis during the campaign.

Species	Limit of detection	Methods	Accuracy
N <sub>2</sub> O <sub>5</sub>	2.7 pptv (1 $\sigma$ , 1 min)	CEAS	$\pm$ 19%
ClNO <sub>2</sub>	16 pptv (2 $\sigma$ , 1 min)	FIGAERO-ToF-CIMS	$\pm$ 23%
NO	60 pptv (2 $\sigma$ , 1 min)	Chemiluminescence	$\pm$ 20%
NO <sub>2</sub>	0.3 ppbv (2 $\sigma$ , 1 min)	Mo convert	$\pm$ 50%
O <sub>3</sub>	0.5 ppbv (2 $\sigma$ , 1 min)	UV photometry	$\pm$ 5%
Aerosol surface area	- (4 min)	SMPS, APS	$\pm$ 30%
VOCs	0.1 ppbv (5 min)	PTR-MS	$\pm$ 30%
PM <sub>2.5</sub>	0.1 $\mu\text{g m}^{-3}$ (1 min)	TEOM	$\pm$ 5%
PM <sub>1.0</sub> components	0.15 $\mu\text{g m}^{-3}$ (4 min)	HR-ToF-AMS	$\pm$ 30%

820

821 **Table 2.** Summary of the field observed ambient ClNO<sub>2</sub>/N<sub>2</sub>O<sub>5</sub>.

Location	Region	ClNO <sub>2</sub> /N <sub>2</sub> O <sub>5</sub> <sup>a</sup>	References
Beijing, China	Inland	0.7 – 42.0 (5.4)	This work
Wangdu, China	Inland	0.4 - 131.3 (29.5)	Tham et al., 2016
Jinan, China	Marine	25.0 - 118.0 <sup>b</sup>	X. F. Wang et al., 2017
Mt. Tai, China	Marine	~ 4.0	Z. Wang et al., 2017
Hong Kong, China	Marine	0.1 - 2.0	T. Wang et al., 2016
London, UK	Inland	0.02 - 2.4 (0.51)	Bannan et al., 2015
Frankfurt, Germany	Inland	0.2 - 3.0	Phillips et al., 2012
Colorado, USA	Inland	0.2 - 3.0	Thornton et al., 2010
California, USA	Marine	~ 0.2 - 10.0 <sup>c</sup>	Mielke et al., 2013

822 Note: <sup>a</sup> Daily average results; <sup>b</sup> Power plant plume cases at Mt. Tai in Shandong, China; <sup>c</sup> Estimated according to Mielke  
823 et al., (2013).

824

**Table 3.** Summary of the average  $\gamma \times f$  values derived in the field observations.

Location	Region	$\gamma \times f$	References
Beijing, China	suburban	$0.019 \pm 0.009$	This work
Frankfurt, Germany	suburban	0.014	Phillips et al., 2016
Mt. Tai, China	suburban	0.016	Z. Wang et al., 2017
Jinan, China	urban	<0.008	X. F. Wang et al., 2017
California, USA	urban	0.008	Mielke et al., 2013

825

826

**Table 4.** List of the  $\text{N}_2\text{O}_5$  uptake coefficients and the yield of  $\text{ClNO}_2$  in this campaign.

Start time	End time	$\gamma$	$f$
05/25 00:00	05/25 05:00	$0.047 \pm 0.023$	$0.60 \pm 0.30$
05/25 18:30	05/25 23:00	$0.012 \pm 0.006$	$1.0 \pm 0.50$
05/27 19:00	05/27 20:40	$0.040 \pm 0.032$	$0.50 \pm 0.40$
05/28 19:00	05/28 23:00	$0.017 \pm 0.009$	$1.0 \pm 0.50$
05/30 21:00	05/31 00:00	$0.055 \pm 0.030$	$0.55 \pm 0.30$

827